

Robust tuning of feedback linearizing controllers via bifurcation analysis

Juergen Hahn^{1,2}, Martin Mönnigmann², and Wolfgang Marquardt²

¹Department of Chemical Engineering
Texas A&M University
College Station, Texas

²Lehrstuhl für Prozesstechnik
RWTH Aachen
Germany

Abstract

Feedback linearization is a nonlinear controller design strategy that results in an explicit formulation of the feedback control law. This method can result in excellent performance if an accurate dynamic process model is available. However, feedback linearization suffers from a lack of robustness if plant-model mismatch exists. The approach presented in this work analyzes the robustness properties of the closed-loop process with specific regard to the controller tuning parameter. Due to this, it is possible to tune the controller such that robustness over the entire operating region is guaranteed even under the assumption of certain types of model mismatch. This method is illustrated with an example and conclusions about its applicability to more general model and controller formulations are presented.

1 Introduction

Nonlinear process control has become increasingly popular in the chemical process industries. This is due to the trend towards speciality products, tighter profit margins, more stringent environmental requirements, as well as advances in nonlinear systems theory and in the numerical implementation of nonlinear controllers (Bequette, 1991).

Feedback linearization is a nonlinear controller design technique that can result in excellent performance if an accurate model of the process is known. However, the closed-loop performance can degrade significantly, even up to the point that the process can become unstable, if the real model contains inaccuracies in the parameters or includes unmodeled dynamics (Henson and Seborg, 1991). There are several possibilities to circumvent this:

- A simpler controller could be used. This approach can increase the robustness but will usually decrease controller performance, especially when the operating region of the process is large.
- A robust nonlinear controller could be designed.

However, this will result in controllers that are even more complicated to design, implement, and maintain than regular feedback linearizing controllers.

This paper presents a different approach of dealing with model mismatch for nonlinear controller design. The model and its uncertainties are thoroughly analyzed by performing bifurcation analysis on the closed-loop system. Subsequently, the results from this analysis are used to tune the controller. In particular, it is often possible to tune a feedback linearizing controller such that robust stability is guaranteed.

The procedure is illustrated using an unstable reactor as an example. For this case study, uncertainty in the model parameters will result in an upper bound on the controller tuning parameter, while unmodeled dynamics will result in a lower bound. This upper and lower bound on the tuning parameter correspond to, roughly speaking, a lower and an upper bound on the aggressiveness of the controller. From the bifurcation analysis it can be inferred that the controller will guarantee robust stability over the entire operating region for tuning parameter values between these bounds. In addition to robustness, it is also possible to use these bounds in order to achieve good performance even if there exists mismatch between the real model and the one that is used for designing the controller.

2 Feedback Linearization

Two main categories of designing controllers via feedback linearization can be identified: input-output linearization and state-space linearization. The presentation in this paper will exclusively focus on the former because it is more generally applicable and will result in linear input-output behavior of the system if no model mismatch is present.

Consider a single-input single-output (SISO) nonlinear system with n states of the form

$$\begin{aligned}\dot{x}(t) &= f(x(t)) + g(x(t))u(t) \\ y(t) &= h(x(t)).\end{aligned}\tag{1}$$

If this system has a well-defined relative degree r then it can be transformed into normal form via a diffeomorphism $[\xi^T, \eta^T]^T = \Phi(x)$. The ξ coordinates are defined as

$$\xi_k = \Phi_k(x) = L_f^{k-1}h(x), \quad 1 \leq k \leq r \quad (2)$$

and the $\eta_j = \Phi_{r+j}(x), 1 \leq j \leq n - r$ (Isidori, 1995; Kravaris and Kantor, 1990) correspond to the internal dynamics of the closed-loop process. The normal form of the system is then given by

$$\begin{aligned} \dot{\xi}_1 &= \xi_2 \\ \dot{\xi}_2 &= \xi_3 \\ &\vdots \\ \dot{\xi}_r &= L_f^r h(x) + L_g L_f^{r-1} h(x)u \\ \dot{\eta} &= q(\xi, \eta) \\ y &= \xi_1 \end{aligned} \quad (3)$$

The map between the input and the output can be linearized by choosing a static state feedback control law

$$u = \frac{v - L_f^r h(x)}{L_g L_f^{r-1} h(x)} \quad (4)$$

such that the r -th equation of (3) becomes $\dot{\xi}_r = v$. It is possible to place the poles of the closed-loop transfer function for the linearized subsystem ξ in the complex plane by choosing an appropriate feedback v . For the purpose of this paper only one tuning parameter, ϵ , which represents the time constant of the closed-loop system is used to shape the closed-loop response. A feedback linearizing controller in terms of the original states is then given by

$$u = \frac{-L_f^r h(x) - \frac{\binom{r}{r-1}}{\epsilon} L_f^{r-1} h(x) - \dots - \frac{\binom{r}{1}}{\epsilon^{r-1}} L_f h(x)}{L_g L_f^{r-1} h(x)} + \frac{\frac{1}{\epsilon^r} (y_{sp} - h(x))}{L_g L_f^{r-1} h(x)} \quad (5)$$

When this control law is applied to the process, the closed-loop transfer function between the system output y and the set point y_{sp} becomes

$$\frac{y}{y_{sp}} = \frac{1}{(\epsilon s + 1)^r} \quad (6)$$

under the assumption that $y(0) = y_{sp}(0)$.

It is also possible to include integral action in the controller in order to compensate for possible inaccuracies in the model. The feedback linearizing controller with integral action is given by

$$u = \frac{-L_f^r h(x) - \frac{\binom{r+1}{r}}{\epsilon} L_f^{r-1} h(x) - \dots - \frac{\binom{r+1}{2}}{\epsilon^{r-1}} L_f h(x)}{L_g L_f^{r-1} h(x)} + \frac{\frac{\binom{r+1}{1}}{\epsilon^r} (y_{sp} - h(x)) + \frac{1}{\epsilon^{r+1}} \int_0^t (y_{sp} - h(x)) d\tau}{L_g L_f^{r-1} h(x)} \quad (7)$$

resulting in the closed-loop transfer function

$$\frac{y}{y_{sp}} = \frac{(r+1)\epsilon s + 1}{(\epsilon s + 1)^{r+1}} \quad (8)$$

under the condition that $y(0) = y_{sp}(0)$.

The transfer functions shown in equations (6) and (8) only represent the closed-loop system behavior if the matching conditions are satisfied up to a degree of at least r . Since this investigation specifically focuses on controller tuning under the influence of model mismatch, the controller implementation shown in equation (7) will be used. Due to the model mismatch it will not be possible to exactly achieve the closed-loop response shown in equation (8). However, the integrating term in the controller will ensure that the desired set point can be reached and appropriate tuning of the controller can still result in good performance for many cases.

For the implementation of feedback linearizing controllers it is usually postulated that the internal dynamics of the process is stable and that the values of the states are exactly known. While this investigation also uses the latter assumption, it will be shown that the validity of the former assumption can easily be analyzed as part of the proposed tuning method.

3 Bifurcation Analysis

Bifurcation theory allows to systematically identify critical points on the steady state manifold of a parametrized ODE or DAE system. The term critical point refers to a point at which the dynamic behavior of the system changes qualitatively. For example, at Hopf and saddle-node bifurcations, stable and unstable steady states meet. Therefore, stability boundaries in the process parameter space can be investigated by locating these critical points for the system of interest. The use of bifurcation theory in conjunction with parameter continuation is well established. As one-parametric curves of steady states are calculated by parameter continuation, critical points can be detected by monitoring sign changes of appropriate test functions (Beyn *et al.*, 2002). Once a bifurcation point has been detected, a curve of bifurcation points can be calculated by continuation from this point, just as a curve of steady states was calculated starting from a known steady state in the first step. The sequence of continuation, detection of critical points, and subsequent continuation of a critical point can be repeated for critical points of higher order, e.g. for a cusp point found on a curve of saddle-node bifurcations. While many higher order critical points are related to exotic dynamic behavior, some reveal information which can be exploited for engineering purposes. Most notably in the present context, sets of cusp points bound regions of the process parameter space in which no saddle-node

bifurcations occur. Similarly, sets of a particular type of degenerate Hopf point bound regions in which no Hopf points occur. Since Hopf and saddle-node points mark the stability boundary, knowledge about the location of degenerate Hopf and cusp points will be exploited in section 4 to identify regions in which no loss of stability can occur for any value of the parameters. Remarkably, bifurcation analysis has rarely been applied to closed-loop processes to the authors' knowledge (Cibrario and Lévine, 1991; Littleboy and Smith, 1998). The relation of the present paper to bifurcation theory-based design methods will be briefly discussed in section 6.

4 Robust Controller Tuning

During controller tuning a trade-off is always associated with performance and robustness requirements. This is due to the fact that good performance leads to aggressive controllers which will usually result in a decrease in the robustness of the closed-loop process. A balance between these objectives has to be found. Methods for tuning linear controllers are well established (Skogestad and Postlethwaite, 1996) but this is not the case for nonlinear controllers, where performance and robustness cannot easily be quantified.

In the following a methodology for determining upper and lower bounds for tuning parameters for feedback linearizing controllers is presented. This approach is based upon bifurcation analysis of the closed-loop system. The method will be illustrated by an example and a generalization of this tuning method is discussed in the next section.

Consider a continuous stirred tank reactor (CSTR) for an exothermic, irreversible reaction, $A \rightarrow B$ (Uppal *et al.*, 1974). Assuming constant liquid volume, the following dynamic model can be derived based upon a component and an energy balance:

$$\dot{C}_A = \frac{q}{V} (C_{Af} - C_A) - k_0 \exp\left(-\frac{E}{RT}\right) C_A \quad (9)$$

$$\begin{aligned} \dot{T} = \frac{q}{V} (T_f - T) - \frac{\Delta H}{\rho C_p} k_0 \exp\left(-\frac{E}{RT}\right) C_A \\ + \frac{UA}{V\rho C_p} (T_c - T) \quad (10) \end{aligned}$$

The values of the parameters and the nominal operating conditions for this process are shown in Table 1. The temperature of the cooling fluid, T_c , can be manipulated and the reactor temperature, T , is measured. This results in a system consisting of two states with a single input and a single output. The bifurcation diagram of the open-loop system is shown in Figure 1. The equilibria of the system consist of two stable branches and one unstable branch connecting the two

Variable	Value	Variable	Value
q	$100 \frac{L}{min}$	$\frac{E}{R}$	$8750K$
C_{Af}	$1 \frac{mol}{L}$	k_0	$7.2 \cdot 10^{10} \frac{1}{min}$
T_f	$350K$	UA	$5 \cdot 10^4 \frac{1}{minK}$
V	$100L$	T_c	$300K$
ρ	$1000 \frac{g}{L}$	C_A	$0.5 \frac{mol}{L}$
C_p	$0.239 \frac{J}{gK}$	T	$350K$
ΔH	$-5 \cdot 10^4 \frac{J}{mol}$		

Table 1: Parameters for the CSTR

stable ones. The system also has two limit points and one Hopf point. The nominal operating point shown in Table 1 lies on the open-loop unstable branch. When a

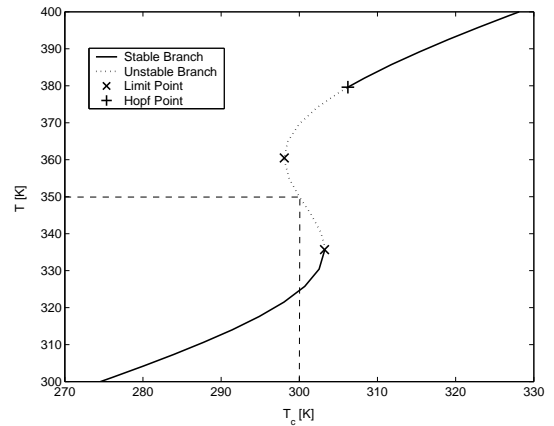


Figure 1: Bifurcation diagram of the open-loop system.

controller like the one given by equation (7) is designed for this process it results in the following feedback control law

$$u = \frac{-\frac{q}{V} (T_f - T) + \frac{\Delta H}{\rho C_p} k_0 \exp\left(-\frac{E}{RT}\right) C_A + \frac{UA}{V\rho C_p} T}{\frac{UA}{V\rho C_p}} + \frac{\frac{2}{\epsilon} (T_{sp} - T) + \frac{1}{\epsilon^2} \int_0^t (T_{sp} - T) d\tau}{\frac{UA}{V\rho C_p}} \quad (11)$$

$$T_c = u \quad (12)$$

Assuming that there is no mismatch between the plant and the model, the controller of the form of equation (11) results in a system that has a stable input-output behavior as well as a stable internal dynamics for any value of ϵ and any set point, T_{sp} , within the operating region. This can easily be verified by applying bifurcation analysis to the closed-loop system. For this nominal case the value of ϵ can be made arbitrarily small, resulting in a very fast response. However, in an on-line application there is always some mismatch between the plant and the model which can also lead to restrictions for the controller tuning.

Assume that the heat transfer coefficient, UA , of the

real plant represented by equation (10) is not identical to the one for the model shown in equation (11) due to uncertainty in this parameter. For the plant a value of UA equal to $5 \cdot 10^4 \frac{J}{\text{min}K}$ is used whereas for the model a value of $5.5 \cdot 10^4 \frac{J}{\text{min}K}$ is assumed. When bifurcation analysis of this closed-loop system is performed, it is found that the system can become unstable for high values of ϵ because there is a Hopf point along the equilibrium curve for some values of T_{sp} . Starting from this Hopf point, a Hopf curve can be computed where both ϵ and T_{sp} are varied. The curve shown in Figure 2 results from this where the shaded region is unstable and the region outside of the Hopf curve corresponds to stable steady states. It can be concluded that the system will always be stable if ϵ is smaller than a certain value corresponding to the peak of the Hopf curve.

Next, it was investigated how this peak moves with

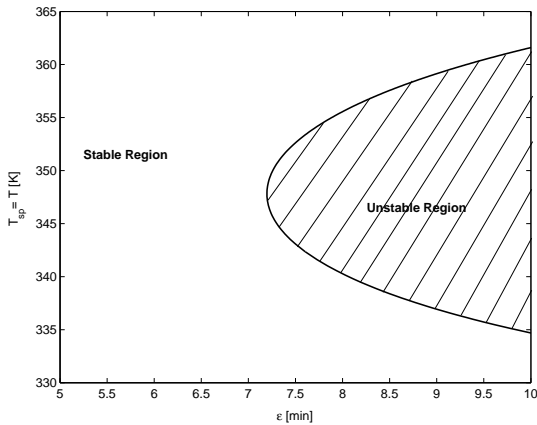


Figure 2: Hopf curve of the closed-loop system for model mismatch in UA of 10%.

variations in the parameter uncertainty. This way it can be established how much the controller can be detuned without losing stability for a specific uncertainty in the model parameter. The corresponding curve is shown in Figure 3. This curve provides information about how large ϵ can be chosen for a certain mismatch in the model parameter in order to guarantee robust stability. If the model mismatch is less than what was assumed for the controller design then the closed-loop system will also be stable. It should be pointed out that values of ϵ that are close to the critical ϵ will usually result in low performance of the closed-loop system. When the model parameter UA is chosen to be less than the real value of the plant ($UA = 5 \cdot 10^4 \frac{J}{\text{min}K}$) then this model mismatch has a stabilizing effect. For such a case any value of ϵ will result in a stable closed-loop system.

Similar investigations have been performed for mismatch in other model parameters ($k_0, \frac{E}{R}$). All of these lead to similar conclusions that there exists an upper bound for the value of ϵ for some form of model mismatch. Tuning the controller more aggressively by

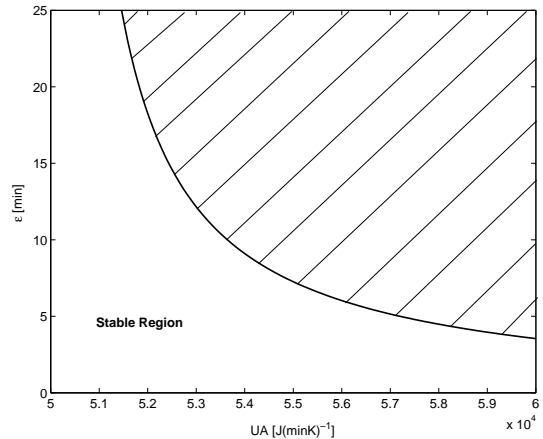


Figure 3: ϵ vs. UA along the peak of the Hopf curve.

choosing a smaller value of ϵ than this bound will guarantee robustness against parameter uncertainty for the investigated case over the entire operating region.

Another form of model mismatch that needs to be considered is unmodeled dynamics. Since no model can describe every detail of a process with perfect precision, it is commonly assumed that the fast dynamics of the process can be neglected. While this is generally a good assumption, it does lead to a bound on the achievable closed-loop performance. For linear controllers the uncertainty can be described in the frequency domain and unmodeled dynamics will result in a large uncertainty weight at high frequencies (Skogestad and Postlethwaite, 1996). Unfortunately, such a characterization of the uncertainty is not possible for nonlinear systems. However, bifurcation analysis can be performed on a system that contains the most important part of the fast dynamics while a controller that has no knowledge about this dynamics is used to control it. For this case study, the plant model is augmented by the following two equations that describe the actuator dynamics as an overdamped second order process

$$\begin{aligned} \epsilon_v \dot{T}_c &= -T_c + z \\ \epsilon_v \dot{z} &= -z + u \end{aligned} \quad (13)$$

where ϵ_v corresponds to the time constant of the cooling system. The equations in (13) replace the original equation (12) for the following investigation. The goal is to tune the controller such that robust stability is guaranteed for this form of model mismatch.

Investigation of the closed-loop system under the assumption of unmodeled dynamics given by equation (13) ($\epsilon_v = 0.02$ min) but no parametric uncertainty shows that the system exhibits a Hopf point when T_{sp} is held constant and ϵ is varied. Computing the Hopf curve by starting from the Hopf point and varying both T_{sp} and ϵ results in the curve shown in Figure 4. This figure reveals that the unmodeled dynamics results in a lower bound on the controller tuning parameter, ϵ , for any fixed value of T_{sp} . Since the curve shown in Figure

4 has a peak at about $\epsilon = 0.055$ min, robust stability can be guaranteed for any T_{sp} by setting $\epsilon > 0.055$ min. Figure 5 shows how the peak on the Hopf curve moves with a variation of the time constant of the unmodeled dynamics, ϵ_v . If ϵ is chosen to be greater than a certain

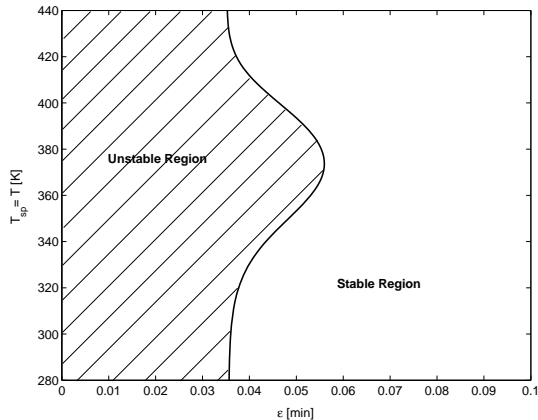


Figure 4: Hopf curve of the closed-loop system for unmodeled dynamics with $\epsilon_v = 0.02$ min.

value for a specific ϵ_v , then the system will be stable over the entire operating region. It can also be concluded that the closed-loop system will be stable for any value of ϵ_v that is smaller than the one that was used for the design. In summary, there are upper and

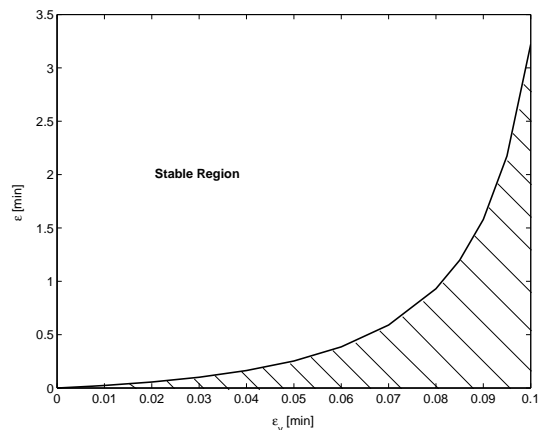


Figure 5: ϵ vs. ϵ_v along the peak of the Hopf curve.

lower bounds for the controller tuning parameter ϵ for this case study. The upper bound results from uncertainty in the model parameters while the lower bound is caused by unmodeled dynamics.

In a final step, the effect of parameter uncertainties on the location of the lower bound for ϵ and the effect of unmodeled dynamics on the location of the upper bound for ϵ are investigated. The existence of unmodeled dynamics has a very mild stabilizing effect on the system for high values of ϵ because the unstable region shown in Figure 2 is moved further to the right when the value of ϵ_v is increased. A similar effect is taking

place for the lower bound of ϵ when UA for the model is chosen to be larger than the parameter in the model because this will move the unstable region in Figure 4 further to the left. However, if the value of UA in the model underestimates the real value of the parameter then the unstable region in Figure 4 will move slightly to the right.

Summarizing, it can be stated that the value of the controller tuning parameter ϵ for the worst case scenario of 1) uncertainty in the parameter UA of up to $\pm 10\%$ 2) unmodeled dynamics of the form of equation (13) with $\epsilon_v \leq 0.02$ min can be determined from the diagram shown in Figure 6. Any value of ϵ between the peak values of 0.059424 min and 7.1969 min will result in robust stability of the closed-loop system over the entire operating region and for any plant model mismatch as described. In order to achieve good per-

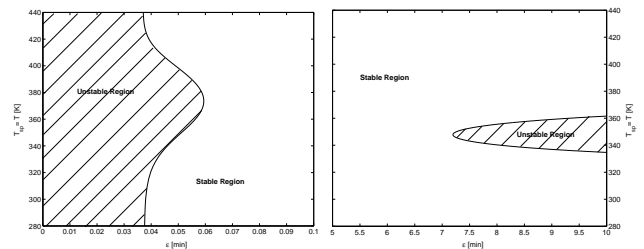


Figure 6: Regions of stability based upon the controller tuning parameter ϵ .

formance in addition to robustness it is recommended to use a value of ϵ that does not lie directly on the stability boundary (e.g. $\epsilon = 0.25$ min for this case). If there is a gap of several orders of magnitude between the smallest and the largest value of the tuning parameter then it is recommended to stay closer to the lower value in order to achieve a faster response. Ultimately, the dynamics of the open-loop process has also to be considered for tuning the controller.

All of the results derived from bifurcation analysis have been confirmed in simulations with the dynamic system.

5 Controller Tuning Procedure

The previous section illustrated the controller tuning method by applying it to a specific example. However, the same tuning method can be applied to processes in general. It contains no restriction about the process to be controlled or the type of controller to be tuned. For feedback linearizing controllers the following steps should be included in the controller tuning process:

1. Design and implement the controller on the simulated process.
2. Analyze the internal dynamics of the closed-loop

system using bifurcation analysis. This should be performed at the operating point as well as over the entire operating region in order to determine if the internal dynamics will remain stable over this region.

3. Tune the controller to satisfy a nominal performance requirement. This is trivial to do for the nominal case because the input-output behavior of the closed-loop process corresponds to equation (6) or (8) if a controller of the type of equation (5) or (7) is being used.
4. Identify the main sources of parametric uncertainty in the model. Subsequently, analyze the closed-loop system using bifurcation analysis under the assumption of parametric uncertainty. This can result in restrictions on the controller tuning parameters.
5. Perform bifurcation analysis on the closed-loop system under the assumption of unmodeled dynamics. This investigation might place further bounds on the controller tuning parameters.
6. Investigate the region for the controller tuning parameters for which the closed-loop system remains stable under the worst possible combination of parametric uncertainty and unmodeled dynamics over the entire operating region. This is an important point in order to guarantee robust stability of the controller.
7. If the controller tuning parameters that satisfy the nominal performance requirement can also guarantee robust stability then they can be kept. Otherwise, the controller has to be retuned in order to guarantee robust stability. It should be pointed out that it is desirable to use controller tuning parameters that do not lie close to a region of instability of the closed-loop process in order to also achieve good robust performance.

It is stressed that step 6 of the above procedure corresponds to an analysis of cusp and degenerate Hopf points involving more than two parameters. Figure 6, for example, was obtained by locating a degenerate Hopf point from Figure 4 and Figure 2 in three parameters by repeatedly calculating curves in two parameters for a variety of fixed values of the third parameter. Repeated calculation of curves in two parameters will become tedious if extremal points must be found w.r.t. more than three parameters. It is worth noting that bifurcation theory-based design methods (Mönnigmann and Marquardt, 2002) are available which can deal with a larger number of parameters than bifurcation analysis.

Following these steps will result in a controller that is tuned such that it meets nominal stability, nominal performance, as well as robust stability requirements.

6 Conclusions

This paper presented a controller tuning strategy for nonlinear systems. The method is based upon applying bifurcation analysis to the closed-loop system in order to determine regions of stability for the controller tuning parameters. It is often possible to tune the controller such that it meets nominal performance as well as robust stability requirements. This approach was illustrated by tuning a feedback linearizing controller for an unstable nonlinear plant, under the assumption of parametric uncertainty as well as unmodeled dynamics. However, the approach as such can also be applied to different types of controllers, plants with different characteristics, as well as under the assumption of different types of plant-model mismatch.

References

- Bequette, B.W. (1991). Nonlinear control of chemical processes: A review. *Ind. Eng. Chem. Res.* **30**, 1391–1413.
- Beyn, W.-J., A. Champneys, E. Doedel, W. Govaerts, Yu.A. Kuznetsov and B. Sanstede (2002). Numerical continuation, and computation of normal forms. In: *Handbook of Dynamical Systems* (B. Fiedler, Ed.). Vol. 2. pp. 149–219. Elsevier Science, North-Holland.
- Cibrario, M. and J. Lévine (1991). Saddle-node bifurcation control with application to thermal runaway of continuous stirred tank reactors. In: *Proc. 30th Contr. Decis. Conf.* pp. 1551–1552.
- Henson, M.A. and D.E. Seborg (1991). Critique of exact linearization strategies for process control. *J. Proc. Cont.* **1**, 122–139.
- Isidori, A. (1995). *Nonlinear Control Systems*. Springer-Verlag, New York.
- Kravaris, C. and J.C. Kantor (1990). Geometric methods for nonlinear process control. 2. Controller synthesis. *Ind. Eng. Chem. Res.* **29**, 2310–2323.
- Littleboy, D. M. and P. R. Smith (1998). Using bifurcation methods to aid nonlinear dynamic inversion control law design. *Journal of Guidance, Control, and Dynamics* **21**(4), 632–638.
- Mönnigmann, M. and W. Marquardt (2002). Normal vectors on manifolds of critical points for parametric robustness of equilibrium solutions of ODE systems. *J. Nonlinear Sc.* **12**, 85–112.
- Skogestad, S. and I. Postlethwaite (1996). *Multivariable Feedback Control*. John Wiley, New York.
- Uppal, A., W.H. Ray and A.B. Poore (1974). On the dynamic behavior of continuous stirred tank reactors. *Chem. Eng. Sci.* **29**, 967–985.

CLOSED LOOP PROPERTIES AND BLOCK RELATIVE GAIN

Vinay Kariwala, J. Fraser Forbes and Edward S. Meadows

*Department of Chemical & Materials Engineering
University of Alberta, Edmonton, Alberta, Canada*

Abstract: Block Relative Gain (BRG) is a useful method for screening alternatives for block decentralized control at the design stage. In this paper, we establish the connection between the BRG and closed loop properties like stability, input output controllability, block diagonal dominance and interactions. Based on these results, simple rules for pairing of variables for block decentralized control are proposed.

Keywords: Control System Design, Decentralized control, Interaction.

1. INTRODUCTION

Manousiouthakis *et al.* (1986) generalized the concept of Relative Gain Array (RGA) (Bristol, 1966) to Block Relative Gain (BRG). It is a powerful technique for input-output controllability analysis and screening alternatives for block decentralized control quickly at the design stage. During the past few years, RGA has been studied extensively (Grosdidier *et al.*, 1985; Hovd and Skogestad, 1992) and its properties are well understood, but BRG has largely been overlooked. Some researchers (Nett and Manousiouthakis, 1987; Chen, 1992) have found relations between BRG and Euclidian condition number. It is shown that generally, a system is difficult to control, if the maximum singular value of BRG is large. Despite these studies, BRG has not gained widespread popularity and block pairings are selected primarily based on heuristics (Castro and Doyle, 2002). This can be attributed to lack of studies showing that, similar to RGA, information regarding closed loop properties can be obtained using BRG. This motivates the present work.

In this paper, we establish the connection between BRG and closed loop properties like stability, input output controllability, block diagonal dominance and interactions. We show that the common

conjecture that a system is *weakly* interacting, if BRG is close to the identity matrix, is not true. Further, a system can have large interactions despite BRG being exactly the identity matrix. Based on these insights, simple rules for pairing of variables are proposed.

This paper focuses on extracting useful feedback properties from gain information, since it is often the only reliable information available at design stage (Grosdidier *et al.*, 1985). The discussion is limited to square, stable and linear time invariant (LTI) systems represented as $\mathbf{G}(s)$. The steady state gain matrix is represented as $\mathbf{G}(0)$ or simply $\mathbf{G} \in \mathbb{R}^{n \times n}$ and its individual elements as g_{ij} . A vector of variables is denoted by a boldface letter (e.g. \mathbf{y} , \mathbf{u}). The objective is to decompose the original system into a set of M non-overlapping square subsystems such that, $\mathbf{G}_{ii} \in \mathbb{R}^{m_i \times m_i}$; $i = 1, 2 \dots M$, $\sum_i m_i = n$. The pair $(\mathbf{y}_i, \mathbf{u}_j)$ denotes the variables related by $\mathbf{G}_{ij}(s)$, which is the ij^{th} block of $\mathbf{G}(s)$.

2. PRELIMINARIES

Let the system be partitioned as shown in Figure 1. The steady state BRG between $(\mathbf{y}_1, \mathbf{u}_1)$ is defined as (Manousiouthakis *et al.*, 1986),

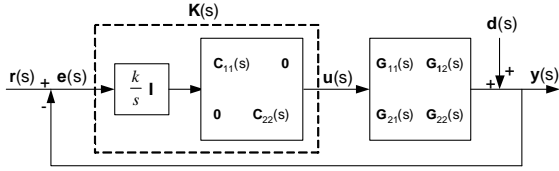


Fig. 1. Block Diagram of Closed loop system

$$[\mathbf{\Lambda}_B]_{11} = \mathbf{G}_{11}[\mathbf{G}^{-1}]_{11} \quad (1)$$

where \mathbf{G}_{11} and $[\mathbf{G}^{-1}]_{11}$ are the first $m_1 \times m_1$ blocks of \mathbf{G} and \mathbf{G}^{-1} respectively. If, \mathbf{G}_{22} is non-singular, then recognizing that $[\mathbf{G}^{-1}]_{11} = \bar{\mathbf{G}}_{11}^{-1}$, $[\bar{\mathbf{G}}]_{11} = \mathbf{G}_{11} - \mathbf{G}_{12}\mathbf{G}_{22}^{-1}\mathbf{G}_{21}$ (Horn and Johnson, 1990), the BRG between $(\mathbf{y}_1, \mathbf{u}_1)$ can be alternatively calculated as

$$[\mathbf{\Lambda}_B]_{11} = \mathbf{G}_{11}\bar{\mathbf{G}}_{11}^{-1} \quad (2)$$

Similarly, the BRG between $(\mathbf{y}_i, \mathbf{u}_i)$ can be defined as

$$[\mathbf{\Lambda}_B]_{ii} = \mathbf{G}_{ii}[\mathbf{G}^{-1}]_{ii} = \mathbf{G}_{ii}\bar{\mathbf{G}}_{ii}^{-1} \quad (3)$$

Manousiouthakis *et al.* (1986) have suggested choosing the pairings such that the eigenvalues of $[\mathbf{\Lambda}_B]_{ii}$ are close to 1 for all i . This rule is based on the incorrect conjecture that a system is *weakly* interacting if the BRG is close to the identity matrix. Due to this limitation, this rule can lead to pairings with significant interactions in many cases.

3. CLOSED LOOP PROPERTIES

3.1 Stability

In this section, we establish the connection between the BRG and simultaneous stabilization of the closed loop system and individual loops. It is based on a similar result for RGA shown to be true by Grosdidier *et al.* (1985).

Let the system $\mathbf{G}(s)$ be partitioned as shown in Figure 1. If the controller contains an integrating element to give asymptotically zero tracking error, $\mathbf{K}_{ii}(s)$ can be expressed as $\frac{k}{s}\mathbf{C}_{ii}(s)$, $k > 0$. It is assumed that $\mathbf{C}_{ii}(s)$ and $\mathbf{G}_{ii}(s)$ are stable, contain no transmission zeros and $\mathbf{G}(s)\mathbf{C}(s)$ is proper. Defining, $\mathbf{L}(s) = \mathbf{G}(s)\mathbf{K}(s)$, the closed loop system is given by

$$\mathbf{y}(s) = [\mathbf{I} + \mathbf{L}(s)]^{-1}\mathbf{L}(s)\mathbf{r}(s) + [\mathbf{I} + \mathbf{L}(s)]^{-1}\mathbf{d}(s)$$

and $\mathbf{y}_1(s)$ is given by

$$\begin{aligned} \mathbf{y}_1(s) = & \left[\hat{\mathbf{L}}_{11}(s)\mathbf{L}_{11}(s) + \hat{\mathbf{L}}_{12}(s)\mathbf{L}_{21}(s) \right] \mathbf{r}_1(s) \\ & + \left[\hat{\mathbf{L}}_{11}(s)\mathbf{L}_{12}(s) + \hat{\mathbf{L}}_{12}(s)\mathbf{L}_{22}(s) \right] \mathbf{r}_2(s) \\ & + \hat{\mathbf{L}}_{11}(s)\mathbf{d}_1(s) + \hat{\mathbf{L}}_{12}(s)\mathbf{d}_2(s) \end{aligned} \quad (4)$$

where $\hat{\mathbf{L}}_{ij}(s) = [\mathbf{L}^{-1}(s)]_{ij}$. Using the property of partitioned matrices (Horn and Johnson, 1990):

$$\begin{aligned} \hat{\mathbf{L}}_{11}(s) = & [(\mathbf{I} + \mathbf{L}_{11}(s)) - \mathbf{L}_{12}(s) \\ & (\mathbf{I} + \mathbf{L}_{22}(s))^{-1}\mathbf{L}_{21}(s)]^{-1} \\ \hat{\mathbf{L}}_{12}(s) = & (\mathbf{I} + \mathbf{L}_{11}(s))^{-1}\mathbf{L}_{12}(s)[\mathbf{L}_{21}(s)(\mathbf{I} + \\ & + \mathbf{L}_{11}(s))^{-1}\mathbf{L}_{12}(s) - (\mathbf{I} + \mathbf{L}_{22}(s))]^{-1} \end{aligned}$$

At low frequencies, $[\mathbf{I} + \mathbf{L}_{ij}(s)]^{-1} \approx \mathbf{L}_{ij}^{-1}(s)$ (Hovd and Skogestad, 1992). This approximation is valid, when the controller contains integral action. Using this approximation,

$$\begin{aligned} \hat{\mathbf{L}}_{11}(s) \approx & [\mathbf{I} + \bar{\mathbf{G}}_{11}(s)\mathbf{K}_{11}(s)]^{-1} \\ \hat{\mathbf{L}}_{12}(s) \approx & -\mathbf{L}_{11}^{-1}(s)\mathbf{L}_{12}[\mathbf{I} + \bar{\mathbf{G}}_{22}(s)\mathbf{K}_{22}(s)]^{-1} \end{aligned}$$

where $\bar{\mathbf{G}}_{11}(s)$ and $\bar{\mathbf{G}}_{22}(s)$ represent Schur complements of $\mathbf{G}_{22}(s)$ and $\mathbf{G}_{11}(s)$ in $\mathbf{G}(s)$ respectively. If any of the zeros of $[\mathbf{I} + \bar{\mathbf{G}}_{11}(s)\mathbf{K}_{11}(s)]$ lie in the right half plane and no pole-zero cancellations occur in (4), then the closed loop system is unstable. Similarly, it can be shown that if the system is to be decomposed into M blocks, the stability of system depends on the location of zeros of $[\mathbf{I} + \bar{\mathbf{G}}_{ii}(s)\mathbf{K}_{ii}(s)]$, $i = 1, 2 \dots M$. Now, we can relate this finding to BRG using the concept of integral controllability (Grosdidier *et al.*, 1985).

Lemma 1. If $\text{Re}\{\lambda_j(\bar{\mathbf{G}}_{ii}(0)\mathbf{C}_{ii}(0))\} < 0$; $j = 1, 2 \dots m_i$ for some i , then the closed loop system is not integral controllable.

Sketch of Proof. Since $\mathbf{G}(s)$ is stable and $\mathbf{G}_{ii}(s)$ non-singular for all i by assumption, $\bar{\mathbf{G}}_{ii}(s)$ is also stable. Now, Lemma 1 can be shown to be true by following the proof of Theorem 7 of Grosdidier *et al.* (1985).

It should be noted that the low frequency approximation has little effect on the applicability of Lemma 1, since the maximum value of $\bar{\mathbf{G}}_{ii}(s)\mathbf{K}_{ii}(s)$ is seen at origin of s -plane.

Lemma 2. If $\text{Re}\{\lambda_j(\mathbf{G}_{ii}(0)\mathbf{C}_{ii}(0))\} < 0$; $j = 1, 2 \dots m_i$, then the subsystem $(\mathbf{y}_i(s), \mathbf{r}_i(s))$, considered in isolation, is not integral controllable.

PROOF. If all other loops are open, the stability of subsystem $(\mathbf{y}_i(s), \mathbf{r}_i(s))$ depends on the zeros of $[\mathbf{I} + \mathbf{G}_{ii}(s)\mathbf{K}_{ii}(s)]$. The proof follows by replacing $\bar{\mathbf{G}}_{ii}$ by \mathbf{G}_{ii} in Lemma 1. \square

Proposition 3. If $\det([\mathbf{\Lambda}_B(0)]_{ii}) < 0$, then one of the following is true,

- (1) The i^{th} loop by itself is unstable or
- (2) The closed loop system is unstable.

PROOF. Using (3),

$$\det([\mathbf{A}_B(0)]_{ii}) = \frac{\det(\mathbf{G}_{ii}(0))}{\det(\bar{\mathbf{G}}_{ii}(0))} = \frac{\det(\mathbf{G}_{ii}(0)\mathbf{C}_{ii}(0))}{\det(\bar{\mathbf{G}}_{ii}(0)\mathbf{C}_{ii}(0))}$$

Thus, $\det([\mathbf{A}_B(0)]_{ii}) < 0$, if $\det(\mathbf{G}_{ii}(0)\mathbf{C}_{ii}(0)) < 0$ or $\det(\bar{\mathbf{G}}_{ii}(0)\mathbf{C}_{ii}(0)) < 0$. If $\det(\mathbf{G}_{ii}(0)\mathbf{C}_{ii}(0)) < 0$, then at least one of the eigenvalues of $\mathbf{G}_{ii}(0)\mathbf{C}_{ii}(0)$ is negative since,

$$\det(\bar{\mathbf{G}}_{ii}(0)\mathbf{C}_{ii}(0)) = \prod_{j=1}^{m_i} \lambda_j(\bar{\mathbf{G}}_{ii}(0)\mathbf{C}_{ii}(0))$$

The closed loop system is unstable, if any eigenvalue of $\mathbf{G}_{ii}(0)\mathbf{C}_{ii}(0)$ is negative (see Lemma 1). Similarly, the i^{th} loop, considered in isolation with other loops, is unstable if $\det(\mathbf{G}_{ii}(0)\mathbf{C}_{ii}(0)) < 0$ (see Lemma 2). \square

Proposition 3 can be interpreted on similar terms as Theorem 6 of Grosdidier *et al.* (1985), where the implications of negative RGA elements were drawn. If $\det([\mathbf{A}_B(0)]_{ii}) < 0$ for some i and a controller exists, which stabilizes the individual loops, then the closed loop system is unstable. If the controller is designed such that the closed loop system is stable, then the i^{th} loop is unstable. In this case, the system is loop failure sensitive.

Proposition 3 provides only a necessary condition for stability. Consider the case when the sum of the number of negative eigenvalues of $\bar{\mathbf{G}}_{ii}(0)\mathbf{C}_{ii}(0)$ and $\mathbf{G}_{ii}(0)\mathbf{C}_{ii}(0)$ is even. Then, $\det([\mathbf{A}_B]_{ii})$ will be positive, despite the closed loop system and the individual loop being unstable.

Remark 4. The elements of the BRG with only 1×1 blocks are same as the diagonal elements of the RGA (Manousiouthakis *et al.*, 1986). Thus, Proposition 3 generalizes Bristol's pairing rule of avoiding pairing on negative RGA elements to block pairings.

3.2 Input-Output Controllability

It is well known that Right Half Plane (RHP) zeros pose a limitation on the achievable performance of the system. Hovd and Skogestad (1992) have shown that the frequency dependent RGA can be used to detect the presence of RHP zeros. The applicability of their result is limited to the individual elements of the system and $(n-1) \times (n-1)$ subsystems of $\mathbf{G}(s)$. The next proposition complements their result for subsystems having different dimensions.

Proposition 5. Consider the partition of the system matrix $\mathbf{G}(s)$ as shown in Figure 1. Then $[\mathbf{A}_B(s)]_{11}$ is an $m_1 \times m_1$ transfer function matrix. If there exists m_1 , $2 \leq m_1 \leq n-2$, such that $\lim_{s \rightarrow j\infty} \det([\mathbf{A}_B(s)]_{11})$ is nonzero, finite and has

a different sign from $\det([\mathbf{A}_B(0)]_{11})$, then at least one of the following is true,

- (1) $\mathbf{G}_{11}(s)$ has an RHP transmission zero.
- (2) $\mathbf{G}_{22}(s)$ has an RHP transmission zero.

PROOF. For a given partitioning of the system, $2 \leq m_1 \leq n-2$, consider that $\lim_{s \rightarrow j\infty} \det([\mathbf{A}_B(s)]_{11})$ is nonzero and finite. If the signs of $\det([\mathbf{A}_B(0)]_{11})$ and $\lim_{s \rightarrow j\infty} \det([\mathbf{A}_B(s)]_{11})$ are different, then there exists a frequency ω_o , $\omega_o > 0$, such that $\det([\mathbf{A}_B(j\omega_o)]_{11}) = 0$.

The equality, $\det([\mathbf{A}_B(s)]_{11}) = 0$, is satisfied, iff one or both of $\det(\mathbf{G}_{11}(j\omega_o))$ and $\det(\bar{\mathbf{G}}_{11}^{-1}(j\omega_o))$ are zero. Now, $\det(\mathbf{G}_{11}(j\omega_o))$ being zero implies the presence of an RHP transmission zero in $\mathbf{G}_{11}(s)$ at that frequency. If $\det(\bar{\mathbf{G}}_{11}^{-1}(j\omega_o)) = 0$, then $\bar{\mathbf{G}}_{11}^{-1}(s)$ contains an RHP transmission zero and $\bar{\mathbf{G}}_{11}(s)$ contains an RHP pole at that frequency. Due to stability assumptions, an RHP pole in $\bar{\mathbf{G}}_{11}(s)$ at $s = j\omega_o$ can arise only due to an RHP zero in $\mathbf{G}_{22}(s)$ at $s = j\omega_o$. \square

Manousiouthakis *et al.* (1986) have shown that BRG is input scaling independent. Thus, if an input channel of $\mathbf{G}(s)$ contains an RHP zero, the signs of $\det([\mathbf{A}_B(j\infty)]_{11})$ and $\det([\mathbf{A}_B(0)]_{11})$ will remain unchanged. The change of sign of $\det([\mathbf{A}_B(s)]_{11})$ is only a sufficient, but not a necessary condition for the presence of RHP zeros in the subsystems of $\mathbf{G}(s)$.

Proposition 5 excludes the case in which any subsystem contains a zero at the origin, ($s = 0$). Should a subsystem contain a zero at the origin, it would be extremely difficult to control the system. The relation between zeros at the origin and the steady state BRG is established in the next corollary. The proof of this corollary follows directly from the proof of Proposition 5.

Corollary 6. If there exists m_1 , $1 < m_1 < n-1$, such that $\det([\mathbf{A}_B(0)]_{11}) = 0$, then one or both of the subsystems, $\mathbf{G}_{11}(s)$ and $\mathbf{G}_{22}(s)$ contain a zero or a transmission zero at the origin.

Either of these conditions is undesirable, as it makes the subsystem uncontrollable using a controller with integral action. The system may also contain zeros close to the origin in the open left half plane (LHP). Presence of such poorly damped zeros also affects the controllability.

The gain of a multivariate system depends on the input direction. Let the gain of $(\mathbf{y}_1(s), \mathbf{u}_1(s))$ be $\|\mathbf{G}_{11}(0)\mathbf{v}\|_2$, $\|\mathbf{v}\|_2 = 1$. Similarly, let the apparent gain of this loop, when all other loops are closed be $\|\bar{\mathbf{G}}_{11}(0)\mathbf{w}\|_2$, $\|\mathbf{w}\|_2 = 1$.

Proposition 7. The worst case gain mismatch between $\mathbf{G}_{11}(0)$ and $\bar{\mathbf{G}}_{11}(0)$ is bounded as follows,

$$\bar{\sigma}([\mathbf{\Lambda}_B(0)]_{11}) \leq \max_{\substack{\|\mathbf{v}\|_2=1 \\ \|\mathbf{w}\|_2=1}} \frac{\|\mathbf{G}_{11}(0)\mathbf{v}\|_2}{\|\bar{\mathbf{G}}_{11}(0)\mathbf{w}\|_2} \quad (5)$$

$$\frac{1}{\underline{\sigma}([\mathbf{\Lambda}_B(0)]_{11})} \leq \max_{\substack{\|\mathbf{v}\|_2=1 \\ \|\mathbf{w}\|_2=1}} \frac{\|\bar{\mathbf{G}}_{11}(0)\mathbf{w}\|_2}{\|\mathbf{G}_{11}(0)\mathbf{v}\|_2} \quad (6)$$

PROOF. For (5),

$$\begin{aligned} \max \frac{\|\mathbf{G}_{11}(0)\mathbf{v}\|_2}{\|\bar{\mathbf{G}}_{11}(0)\mathbf{w}\|_2} &= \frac{\bar{\sigma}(\mathbf{G}_{11}(0))}{\underline{\sigma}(\bar{\mathbf{G}}_{11}(0))} \\ &= \bar{\sigma}(\mathbf{G}_{11}(0))\bar{\sigma}(\bar{\mathbf{G}}_{11}^{-1}(0)) \\ &\geq \bar{\sigma}([\mathbf{\Lambda}_B(0)]_{11}) \end{aligned}$$

For (6),

$$\begin{aligned} \max \frac{\|\bar{\mathbf{G}}_{11}(0)\mathbf{w}\|_2}{\|\mathbf{G}_{11}(0)\mathbf{v}\|_2} &= \frac{\bar{\sigma}(\bar{\mathbf{G}}_{11}(0))}{\underline{\sigma}(\mathbf{G}_{11}(0))} \\ &= \bar{\sigma}(\bar{\mathbf{G}}_{11}(0))\bar{\sigma}(\mathbf{G}_{11}^{-1}(0)) \\ &\geq \bar{\sigma}([\mathbf{\Lambda}_B(0)]_{11}^{-1}) \\ &\geq \frac{1}{\underline{\sigma}([\mathbf{\Lambda}_B(0)]_{11})} \quad \square \end{aligned}$$

Proposition 7 suggests that if at least one of the conditions, $\bar{\sigma}([\mathbf{\Lambda}_B(0)]_{11}) \gg 1$ and $\underline{\sigma}([\mathbf{\Lambda}_B(0)]_{11}) \ll 1$, is satisfied, then the gain of the $(\mathbf{y}_1(s), \mathbf{u}_1(s))$ loop changes considerably due to closure of all the other loops. If $\bar{\sigma}([\mathbf{\Lambda}_B(0)]_{11}) \approx \underline{\sigma}([\mathbf{\Lambda}_B(0)]_{11}) \approx 1$, the change in gain may still be large, as (5) and (6) are lower bounds on the gain mismatch with one of the loops open. This affirms our earlier assertion that if the BRG is far from the identity matrix, the system has large interactions, but the converse is not true. This is further discussed in §3.4.

3.3 Block diagonal dominance

An advantage of block decentralized controllers is that if the blocks are weakly interacting, then the individual controllers can be tuned independently of each other. The concept of block diagonal dominance can be used to assess this property of the partitioned system. In this section, the relation between block diagonal dominance and BRG is established.

Let the system matrix $\mathbf{G}(s)$ be split into a block diagonal part, $\mathbf{G}_{bd}(s)$ and an off-block diagonal part, $\mathbf{G}(s) - \mathbf{G}_{bd}(s)$. Furthermore, assume that the controller $\mathbf{K}(s)$ has a block diagonal structure same as $\mathbf{G}_{bd}(s)$. Define $\mathbf{E}(s) = (\mathbf{G}(s) - \mathbf{G}_{bd}(s))\mathbf{G}_{bd}(s)^{-1}$. Then, a system is block diagonal dominant (Grosdidier and Morari, 1986), if

$$\mu_{\Delta}(\mathbf{E}(s)) < 1 \quad (7)$$

where μ_{Δ} is the structured singular value (Skogestad and Postlethwaite, 1996) with Δ having same structure as $\mathbf{G}_{bd}(s)$. Next we show that information regarding block diagonal dominance can be obtained using the BRG.

Proposition 8. For a system partitioned into 2 blocks,

$$\mu_{\Delta}(\mathbf{E}(s)) \geq \sqrt{\left| \frac{1}{\underline{\sigma}([\mathbf{\Lambda}_B(s)]_{ii})} - 1 \right|} \quad (8)$$

PROOF. Consider the system being partitioned as shown in Figure 1. Then,

$$\mathbf{E}(s) = \begin{bmatrix} \mathbf{0} & \mathbf{G}_{12}(s)\mathbf{G}_{22}(s)^{-1} \\ \mathbf{G}_{21}(s)\mathbf{G}_{11}(s)^{-1} & \mathbf{0} \end{bmatrix}$$

Using Theorem 2 of Skogestad and Morari (1988),

$$\begin{aligned} \mu_{\Delta}^2(\mathbf{E}(s)) &= \bar{\sigma}(\mathbf{G}_{12}(s)\mathbf{G}_{22}^{-1}(s))\bar{\sigma}(\mathbf{G}_{21}(s)\mathbf{G}_{11}^{-1}(s)) \\ \mu_{\Delta}^2(\mathbf{E}(s)) &\geq \bar{\sigma}(\mathbf{G}_{12}(s)\mathbf{G}_{22}^{-1}(s)\mathbf{G}_{21}(s)\mathbf{G}_{11}^{-1}(s)) \quad (9) \end{aligned}$$

Using (2),

$$\frac{1}{\underline{\sigma}([\mathbf{\Lambda}_B(s)]_{11})} \leq 1 + \bar{\sigma}(\mathbf{G}_{12}(s)\mathbf{G}_{22}^{-1}(s)\mathbf{G}_{21}(s)\mathbf{G}_{11}^{-1}(s)) \quad (10)$$

Substituting (9) in (10) and rearranging,

$$\mu_{\Delta}(\mathbf{E}(s)) \geq \sqrt{\left| \frac{1}{\underline{\sigma}([\mathbf{\Lambda}_B(s)]_{11})} - 1 \right|} \quad (11)$$

Similarly, (8) can be shown to be true for $[\mathbf{\Lambda}_B(s)]_{22}$. \square

Using (8), it can be shown that,

$$\lim_{\underline{\sigma}([\mathbf{\Lambda}_B(0)]_{ii}) \rightarrow 0} \mu_{\Delta}(\mathbf{E}(0)) = \infty$$

Thus the system in Figure 1 cannot be block diagonal dominant if $\underline{\sigma}([\mathbf{\Lambda}_B(0)]_{ii}) \ll 1$. Though this result is proven for the case, when the system is partitioned into two blocks, numerical evidence suggests that it is true for any partitioning.

3.4 Closed loop Interactions

If $\mathbf{G}(s) = \mathbf{G}_{bd}(s)$ or the system itself is block diagonal, it is trivially *non-interacting*. In this section, such a system is referred to as an *ideal* system. When the controller contains integral action, the sensitivity functions of the actual and ideal systems are related as,

$$\begin{aligned}
\mathbf{S}(s) &\approx \mathbf{S}_{bd}(s)\mathbf{\Gamma}(s) & (12) \\
\mathbf{S}(s) &= (\mathbf{I} + \mathbf{G}(s)\mathbf{K}(s))^{-1} \\
\mathbf{S}_{bd}(s) &= (\mathbf{I} + \mathbf{G}_{bd}(s)\mathbf{K}(s))^{-1}
\end{aligned}$$

where $\mathbf{\Gamma}(s) = \mathbf{G}_{bd}(s)\mathbf{G}(s)^{-1}$ is the Performance Relative Gain Array (PRGA) (Hovd and Skogestad, 1992). Let $\mathbf{\Gamma}(s)$ be expressed through its singular value decomposition as, $\mathbf{\Gamma}(s) = \mathbf{U}(s)\mathbf{\Sigma}(s)\mathbf{V}(s)^T$. Then,

$$\mathbf{\Gamma}(s)\mathbf{v}_i(s) = \sigma_i(s)\mathbf{u}_i(s), \quad \forall i = 1 \cdots n$$

where $\sigma_i(s)$ is the i^{th} singular value and $\mathbf{u}_i(s)$ and $\mathbf{v}_i(s)$ are the corresponding left and right singular vectors, calculated at a particular frequency. Grosdidier (1990) has argued that the exogenous signals oriented in the direction of singular vectors associated with $\bar{\sigma}(\mathbf{\Gamma}(s))$ most adversely affect the closed loop performance and vice versa. Then, a necessary condition for interactions to be minimum is that $\sigma_i(\mathbf{\Gamma}(s)) \approx 1$ for all $i = 1, \cdots n$. Recognizing that $[\mathbf{\Lambda}_B(s)]_{ii} = [\mathbf{\Gamma}(s)]_{ii}$,

$$\bar{\sigma}([\mathbf{\Lambda}_B(s)]_{ii}) \leq \bar{\sigma}(\mathbf{\Gamma}(s)) \quad (13)$$

Therefore, if $\bar{\sigma}([\mathbf{\Lambda}_B(s)]_{ii}) \gg 1$, then $\bar{\sigma}(\mathbf{\Gamma}(s)) \gg 1$. When $[\mathbf{\Lambda}_B(s)]_{ii} = \mathbf{I}$, then $\sigma_j([\mathbf{\Lambda}_B(s)]_{ii}) = 1$ for all $j = 1, \cdots m_i$. Then (13) suggests that $\bar{\sigma}(\mathbf{\Gamma}(s))$ can still be large, despite BRG being exactly the identity matrix.

Based on these observations and Proposition 7, we conclude that the system has large interactions if $\bar{\sigma}(\mathbf{\Lambda}_B(s)) \gg 1$ and $\underline{\sigma}(\mathbf{\Lambda}_B(s)) \ll 1$ or in other words, BRG is very different from the identity matrix, but the converse is not true. Use of PRGA is necessary for drawing any conclusions regarding closed loop interactions. Note that due to the approximation involved (see (12)), this result holds only at low frequencies.

4. ALTERNATE PAIRING RULES

In earlier sections, it was shown that useful information regarding closed loop properties can be extracted using BRG. In this section, we summarize those results in the form of pairing rules.

Pairing Rule 1. Avoid pairing on variables with $\det([\mathbf{\Lambda}_B(0)]_{ii}) \leq 0$ (Proposition 3 and Corollary 6).

Pairing Rule 2. Avoid pairing on variables if $\underline{\sigma}([\mathbf{\Lambda}_B(0)]_{ii}) \ll 1$ for some $i = 1, \cdots M$ (Propositions 7 and 8).

Pairing Rule 3. Prefer pairing on variables for which $\sum_i |\sigma_i(\mathbf{\Gamma}(0)) - 1|$ is small, provided Rules 1 and 2 are satisfied (see §3.4).

These rules are based on gain information only and may suggest inferior pairings for systems containing large time delays. In such cases, if a reliable dynamic model is available, then ensuring that $\sum_i |\sigma_i(\mathbf{\Gamma}(s)) - 1|$ is small up to the crossover frequency is helpful. In addition,

Pairing Rule 4. Avoid pairing on variables with different signs of $\det([\mathbf{\Lambda}_B(0)]_{ii})$ and $\det([\mathbf{\Lambda}_B(j\infty)]_{ii})$ (Proposition 5).

Remark 9. Alternatives satisfying $\mu_{\Delta}(\mathbf{E}(0)) < 1$ also possess the property of decentralized integral controllability (DIC) resulting in easier on-line controller tuning. However, the computational load for calculation of μ is substantial (Skogestad and Postlethwaite, 1996). Then, Pairing Rule 2 can be seen as a pre-screening step resulting in reduced computational load.

Remark 10. Since BRG and PRGA are output scaling dependent, so are its singular values. Therefore, prior to pairing selection, specification of a suitable scaling of system matrix is necessary to avoid ambiguity. A possible approach is to normalize the system matrix such that $\|y_i\| \leq 1$ for all $i = 1, \cdots n$.

Remark 11. These pairing rules equally hold for fully decentralized control structures. For many problems, $\sum_i |\sigma_i(\mathbf{\Gamma}(0)) - 1|$ is small, if the diagonal elements of RGA elements are close to 1. Thus, Bristol's rule of pairing on RGA elements close to 1 is implicit here, but, in general, it is neither necessary nor sufficient for the system to be weakly interacting.

5. NUMERICAL EXAMPLE

Example 12. Consider the 4×4 ALSTOM gasifier system (Dixon *et al.*, 2000). The gasifier is described by 3 linearized state space models of 25th order at 100%, 50% and 0% load conditions. Prior to pairing selection, the outputs of the system are scaled such that $\|y_i\|_2 \leq 1$ at all load conditions.

Screening of various block decentralized alternatives for the system is done such that $\det([\mathbf{\Lambda}_B(0)]_{ii}) > 0$ and $\underline{\sigma}(\mathbf{\Lambda}_B(0)) > 0.1$ at different load conditions. A representative set of alternatives satisfying these conditions is presented in Table 1. The pairings (1, 1)¹ and (1-4, 1-4) contain RHP zeros at $s = 3.3013$ and 3.2879 respectively at 100% load conditions making the use of these alternatives unattractive.

Based on steady state analysis, ((1-2-4, 1-3-4), (3-2)) seems to be the best structure. This was

¹ (1,1) represent the pairing ($\mathbf{y}_1, \mathbf{u}_1$).

Pairing	100% load		0% load		Remarks
	$\min_i \underline{\sigma}([\mathbf{A}_B(0)]_{ii})$	$\sum_i \sigma_i(\mathbf{\Gamma}(0)) - 1 $	$\min_i \underline{\sigma}([\mathbf{A}_B(0)]_{ii})$	$\sum_i \sigma_i(\mathbf{\Gamma}(0)) - 1 $	
(1,1),(2,3),(3,2),(4,4)	0.33	2.96	0.48	3.28	RHP zero
(1-2,1-3),(3,2),(4,4)	0.73	2.41	0.48	1.56	
(1-4,1-4),(2,3),(3,2)	0.17	2.99	0.44	4.15	RHP zero
(1-2,1-3),(3-4,2-4)	0.86	1.83	0.53	1.73	
(1-2-3,1-2-3),(4-4)	0.30	2.99	0.43	1.16	
(1-2-4,1-3-4),(3-2)	0.80	1.86	0.75	1.12	

Table 1. Block decentralized pairings for ALSTOM gasifier system

further confirmed by using frequency-dependent PRGA. It is also seen that this alternative satisfies $\mu_{\Delta}(\mathbf{E}(0)) < 1$ at all load conditions and thus is DIC.

This system has also been analyzed by Chin and Munro (2002) at 100% load conditions, where they have suggested the use of ((1-3-4, 2-3-4), (2-1)). This alternative satisfies Rules 1 and 2 at 100% load conditions, but the relative gain of the pairing (2-1) is negative at 0% load conditions. This shows that this alternative will be loop failure sensitive under varying operating conditions.

6. CONCLUSIONS

The main contributions of this paper include:

- (i) an extension of Bristol's rule of avoiding pairing on negative RGA elements to block pairings (Proposition 3),
- (ii) a connection between Grosdidier's interaction measure and BRG. (Proposition 8),
- (iii) a correction and restatement of the common conjecture that a system is *weakly* interacting, if BRG is close to the identity matrix (§3.4).

The pairing rules proposed in this paper will be helpful in selecting block pairings for the system.

ACKNOWLEDGEMENTS

After submission of the manuscript, we found that Proposition 3 was shown to be true earlier by Grosdidier and Morari (Grosdidier and Morari, 1987). The financial support from *National Sciences and Engineering Research Council of Canada* is gratefully acknowledged.

REFERENCES

- Bristol, E.H. (1966). On a new measure of interaction for multivariable process control. *IEEE Trans. Automat. Contr.* **11**, 133–134.
- Castro, J.J. and F.J. Doyle (2002). Plantwide control of the fiber line in a pulp mill. *Ind. Eng. Chem. Res.* **41**, 1310–1320.
- Chen, J. (1992). Relations between block relative gain and Euclidean condition number. *IEEE Trans. Automat. Contr.* **37**(1), 127–129.
- Chin, C.S. and N. Munro (2002). The analysis and control of the alstom gasifier benchmark problem. *Proceedings of XV IFAC World Congress, Barcelona, Spain*.
- Dixon, R., A.W. Pike and M. S. Donne (2000). The ALSTOM benchmark challenge on gasifier control. *Proc. Instn. Mech. Engrs, Part I, Journal of Systems and Control Engineering* **214**(16), 389–394.
- Grosdidier, P. (1990). Analysis of interaction direction with the singular value decomposition. *Computers chem. Engng.* **14**(6), 687–689.
- Grosdidier, P. and M. Morari (1986). Interaction measures for systems under decentralized control. *Automatica* **22**(3), 309–319.
- Grosdidier, P. and M. Morari (1987). A computer aided methodology for the design of decentralized controllers. *Comput. Chem. Engng.* **11**(4), 423–433.
- Grosdidier, P., M. Morari and B.R. Holt (1985). Closed-loop properties from steady-state gain information. *Ind. Eng. Chem. Fundam.* **24**, 221–235.
- Horn, R.A. and C.R. Johnson (1990). *Matrix Analysis*. Cambridge University Press. Cambridge, UK.
- Hovd, M. and S. Skogestad (1992). Simple frequency dependent tools for control system analysis. *Automatica* **28**, 989–996.
- Manousiouthakis, V., R. Savage and Y. Arkun (1986). Synthesis of decentralized process control structures using the concept of block relative gain. *AIChE J.* **32**(6), 991–1003.
- Nett, C.N. and V. Manousiouthakis (1987). Euclidean condition and block relative gain: Connections, conjectures and clarifications. *IEEE Trans. Automat. Contr.* **32**(5), 405–407.
- Skogestad, S. and I. Postlethwaite (1996). *Multivariable Feedback Control: Analysis and design*. John Wiley & sons. New York.
- Skogestad, S. and M. Morari (1988). Some new properties of the structured singular value. *IEEE Trans. Automat. Contr.* **33**(12), 1151–1154.

A TOOL TO ANALYZE ROBUST STABILITY FOR CONSTRAINED MPC

Lino O. Santos* Lorenz T. Biegler**
José A. A. M. Castro*

* *GEPSI – PSE Group, Departamento de Engenharia Química,
Universidade de Coimbra – Pólo II, Pinhal de Marrocos,
3030 - 290 Coimbra, Portugal. E-mail: lino@eq.uc.pt*
** *Department of Chemical Engineering, Carnegie Mellon
University, Pittsburgh PA 15213, USA. E-mail: bieglert@cmu.edu*

Abstract: A sufficient condition for robust stability of nonlinear constrained Model Predictive Control (MPC) with respect to plant/model mismatch is derived. This work is an extension of a previous study on the unconstrained nonlinear MPC problem, and is based on Nonlinear Programming sensitivity concepts. It addresses the discrete time state feedback problem with all states measured. A strategy to estimate bounds on the plant/model mismatch is proposed, that can be used off-line as a tool to assess the extent of model mismatch that can be tolerated to guarantee robust stability.

Keywords: Model-based control, Modeling errors, Nonlinear models, Nonlinear programming, Predictive control, Robust stability, Sensitivity analysis

1. INTRODUCTION

A prominent aspect of the research in the nonlinear Model Predictive Control (MPC) field is the development of a theoretical analysis framework to study the stability and robustness properties of the closed loop system in the presence of disturbances and modeling errors. A broad review by Mayne et al. (2000) on constrained MPC points out that while research on stability has reached a relatively mature stage, further research is required to develop implementable robust MPC for nonlinear systems.

In this work we develop a framework that can be used to evaluate off-line, the closed-loop robustness of a system with constrained MPC in the presence of plant/model mismatch. It is a direct extension of a previous work on the unconstrained case by Santos and Biegler (1999) for the discrete state feedback problem. Both the plant and model are simulated using nonlinear state space models.

The paper is organized as follows. Section 2 is devoted to preliminary definitions and assumptions on the modeling errors, and to a brief description of the MPC problem. In Section 3, we analyze the convergence of the optimal control problem solution for both the perfect and model mismatch cases, by exploiting the properties of the exact penalty function, and we establish a sufficient condition for robust stability. In Section 4, using nonlinear programming sensitivity concepts, we characterize this sufficient condition for the MPC problem with a general cost function. We further detail this characterization for the case of a quadratic cost function, and we obtain a bound on the plant/model uncertainty. This bound can be estimated through off-line calculations using a procedure that constitutes a tool to analyze robust stability for constrained MPC. These results are illustrated in Section 5 with a simple example. Finally, concluding remarks regarding the analysis of conditions for robust stability of

MPC in the presence of plant/model mismatch are given in Section 6.

2. DEFINITIONS AND NOTATION

For this study we treat only the state feedback case and assume that at every time index k all the states can be measured accurately. We assume the state dynamics of the plant are described by the following nonlinear, continuous-time set of equations:

$$\dot{x}^p = \mathbf{f}^p(x^p, u^p), \quad (1)$$

where $x^p \in \mathbf{R}^{n_s}$ is the vector of states and $u^p \in \mathbf{R}^{n_m}$ is the vector of inputs, with $\mathbf{f}^p : \mathbf{R}^{n_s} \times \mathbf{R}^{n_m} \rightarrow \mathbf{R}^{n_s}$.

The stationary discrete-time counterpart of (1) is

$$x_{k+1}^p = f^p(\Delta t; x_k^p, u_k^p), \quad (2)$$

where Δt is the sampling period and $f^p : \mathbf{R}^{n_s} \times \mathbf{R}^{n_m} \rightarrow \mathbf{R}^{n_s}$. We will drop the Δt for convenience. A model with the same dimension as (2) is considered for the MPC framework:

$$x_{k+1} = f(x_k, u_k), \quad (3)$$

where $x_k \in \mathbf{R}^{n_s}$ is the vector of *nominal* states, u_k is the same vector of inputs as in (2), with $f : \mathbf{R}^{n_s} \times \mathbf{R}^{n_m} \rightarrow \mathbf{R}^{n_s}$. We consider $(x_k^p, u_k^p) = (x_k, u_k) = (0, 0)$ the point at which both the plant and the model operate at steady state, such that $f(0, 0) = f^p(0, 0) = 0$.

As in Keerthi and Gilbert (1988) we also apply the definition of a function belonging to class \mathcal{K}_∞ , along with related assumptions. A function $W(r) : \mathbf{R}_+ \rightarrow \mathbf{R}_+$, $r \in \mathbf{R}_+$, belongs to class \mathcal{K}_∞ if: a) it is continuous; b) $W(r) = 0 \Leftrightarrow r = 0$; c) it is nondecreasing; d) $W(r) \rightarrow \infty$ when $r \rightarrow \infty$. We define $\|\cdot\|$ as the Euclidean norm and assume there exists a modeling bound function $W_m(\|x_k\|) \in \mathcal{K}_\infty$ such that $\|f^p(x_k^p, u_k^p) - f(x_k, u_k)\| \leq W_m(\|x_k\|)$, and positive constants K_m and γ such that

$$W_m(\|x_k\|) = K_m \|x_k\|^\gamma. \quad (4)$$

The MPC problem minimizes

$$\Psi(x_i, \mathbf{s}_i) = \sum_{k=i}^{i+p-1} h(x_k, u_k) + h(x_{i+p}), \quad (5)$$

where $\Psi : \mathbf{R}^{n_s} \times \mathbf{R}^{n_m} \rightarrow \mathbf{R}$, $\Psi(0, 0) = 0$. Here $h(x, u) \in \mathcal{K}_\infty$ is a general cost function, x_i is the initial state vector at the time index i , $i \geq 0$, and \mathbf{s}_i is the solution vector over the predictive horizon, given by

$$\mathbf{s}_i^T = [s_i^T \ s_{i+1}^T \ \cdots \ s_{i+p}^T], \quad (6)$$

where $s_{i+k}^T = [x_{i+k}^T \ u_{i+k}^T]$, $k = 0, 1, \dots, p$. This formulation allows a shorter input horizon m , with $m \leq p$ and $u_k = u_{i+m-1}$, $k = i +$

$m, \dots, i + p$. Traditionally, the decision variables of the MPC problem are the control profiles. In the optimization framework used in this study the state profiles are decision variables as well. It uses a multiple shooting method to solve (3) over the predictive horizon (e.g., Santos et al. (1995); Santos (2001)). State and control constraints over this horizon are included in the MPC formulation, set as lower and upper bounds – subscripts $_{\mathbf{L}}$ and $_{\mathbf{U}}$,

$$b(x_k) = \begin{bmatrix} x_k - x_{\mathbf{U}k} \\ -x_k + x_{\mathbf{L}k} \end{bmatrix} \leq 0, \quad (7)$$

with $k = i + 1, \dots, i + p$, and

$$b(u_k) = \begin{bmatrix} u_k - u_{\mathbf{U}k} \\ -u_k + u_{\mathbf{L}k} \end{bmatrix} \leq 0, \quad (8)$$

with $k = i, \dots, i + m - 1$. We define the vector of inequality constraints of the problem at i as

$$\mathbf{b}(\mathbf{s}_i)^T = \begin{bmatrix} b(x_{i+1})^T \cdots b(x_{i+p-1})^T \\ b(u_i)^T \cdots b(u_{i+m-1})^T \end{bmatrix}. \quad (9)$$

Finally, we impose terminal state constraints $x_{i+p} = 0$, or if we allow $p \rightarrow \infty$ then this constraint is automatically satisfied for a finite value of (5).

We denote by $\mathcal{P}(x_i)$ the MPC problem solved at every time index i , $i \geq 0$, given by

$$\min_{\mathbf{s}_i} \Psi(x_i, \mathbf{s}_i) \quad (10)$$

$$\text{s.t. } \mathbf{c}(x_i, \mathbf{s}_i) = 0 \quad (11)$$

$$\mathbf{b}(\mathbf{s}_i) \leq 0, \quad (12)$$

$$\text{where } \mathbf{c}(x_i, \mathbf{s}_i) = \begin{bmatrix} x_{k+1} - f(x_k, u_k) \\ k = i, \dots, i + p - 1 \\ x_{i+p} \end{bmatrix},$$

with optional constraints added for a shorter input horizon, $m \leq p$. We assume in this analysis that \mathbf{s}_i is a feasible solution for (10–12) and that there exists a sufficiently long (and possibly infinite) horizon that insures an admissible trajectory to satisfy the terminal state constraints and (12).

3. STABILITY ANALYSIS

To extend the analysis made for the unconstrained case (Santos and Biegler, 1999) to (10 – 12) we use an exact penalty formulation as developed by Oliveira and Biegler (1994). This approach converts (10 – 12) to the problem $\mathcal{P}_\rho(x_i)$:

$$\min_{\mathbf{s}_i} \Upsilon(x_i, \mathbf{s}_i, \rho_i) \quad (13)$$

$$\text{s.t. } \mathbf{c}(x_i, \mathbf{s}_i) = 0, \quad (14)$$

$$\text{with } \Upsilon(x_i, \mathbf{s}_i, \rho_i) = \Psi(x_i, \mathbf{s}_i) + P(\mathbf{s}_i, \rho_i), \quad (15)$$

$\Upsilon : \mathbf{R}^{n_s} \times \mathbf{R}^{n_m} \rightarrow \mathbf{R}$, $\Upsilon(0, 0, 0) = 0$, where

$$P(\mathbf{s}_i, \rho_i) = \rho_i \cdot \left\{ \sum_{k=i+1}^{i+p-1} \max\{0, b(x_k)\} + \sum_{k=i}^{i+m-1} \max\{0, b(u_k)\} \right\}, \quad (16)$$

and ρ_i is the penalty parameter. We remark that $P(\mathbf{s}_i, \rho_i)$ is bounded from below by zero as well. An important property that motivates the use of the exact penalty function, is that a sufficient condition to recover the original optimal constrained solution, \mathbf{s}_i^* , is to have a finite penalty parameter with $\rho_i > \|\omega_i^*\|_\infty$, where ω_i^* is the vector of the Lagrange multipliers associated to the inequality constraints from the original problem (Fletcher, 1987). Thus this condition on ρ_i ensures that the control and state profiles do not exceed the region delimited by (7) and (8) over p . We will assume that the parameter ρ_i can be chosen in advance to be sufficiently large, i. e.,

$$\rho \geq \max\{\rho_i\}. \quad (17)$$

Note that if ρ_i cannot be bounded, then $\mathcal{P}(x_i)$ has no feasible solution. Of course, feasible solutions of $\mathcal{P}(x_i)$ cannot be guaranteed and for this reason, a 'reasonable' value can be chosen for ρ so that solutions of $\mathcal{P}_\rho(x_i)$ can be considered even if they cannot always satisfy the bound constraints. To simplify the notation we set

$$\Upsilon^*(x_i) = \Upsilon(x_i, \mathbf{s}_i^*, \rho). \quad (18)$$

3.1 Perfect model case

The essence of our stability analysis follows from familiar arguments developed by Muske and Rawlings (see Mayne et al. (2000)). We first consider the case where the model is perfect and there is no source of disturbances. From the assumptions stated in Section 2, the solution of $\mathcal{P}_\rho(x_i)$ satisfies $(x_k, u_k) = (0, 0)$ for $k \geq i + p$. Hence the locally optimal solution gives

$$\Upsilon^*(x_i) = \sum_{k=i}^{i+p-1} h(x_k^*, u_k^*) + \underbrace{h(x_{i+p}^*)}_{=0} + P(\mathbf{s}_i^*, \rho). \quad (19)$$

Note that we assume the point $(x_k^p, u_k^p) = (x_k, u_k) = (0, 0)$ is within the state and control bound constraints.

Consider now the problem at the next time index, $\mathcal{P}_\rho(x_{i+1})$. Because the model is perfect and there is no source of disturbances, the resulting optimal sequence of $\mathcal{P}_\rho(x_i)$ is a feasible solution for $\mathcal{P}_\rho(x_{i+1})$. Moreover, the objective function at the solution of $\mathcal{P}_\rho(x_{i+1})$ can be no greater than the solution $\mathcal{P}_\rho(x_i)$; the solution of $\mathcal{P}_\rho(x_{i+1})$ can not be worse because now the terminal constraint is only enforced one interval ahead. Therefore

$$\Upsilon^*(x_i) - \Upsilon^*(x_{i+1}) \geq h(x_i, u_i^*, \rho), \quad (20)$$

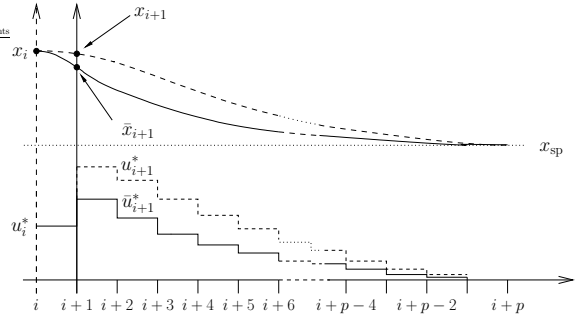


Fig. 1. Plant/Model state trajectory mismatch.

where $h(x_i, u_i^*, \rho) = h(x_i, u_i^*) + \rho \cdot \max\{0, b(x_i)\} + \rho \cdot \max\{0, b(u_i^*)\}$. Note also that $h(x_i, u_i^*, \rho) \in \mathcal{K}_\infty$. Thus the sequence $\{\Upsilon^*(x_i)\}$ over N time indices decreases, and because (5) and (16) are bounded from below by zero it converges. Taking the sum of (20) over N we obtain

$$\Upsilon^*(x_1) - \Upsilon^*(x_{N+1}) = \sum_{i=1}^N (\Upsilon^*(x_i) - \Upsilon^*(x_{i+1})) \geq \sum_{i=1}^N h(x_i, u_i^*, \rho). \quad (21)$$

Also, because $\{\Upsilon^*(x_i)\}$ is decreasing, then as $N \rightarrow \infty$, $h(x_i, u_i^*, \rho) \rightarrow 0$ and $x_i \rightarrow 0$.

3.2 Model mismatch case

Consider now the case with plant/model mismatch. Again, suppose that the solution of $\mathcal{P}_\rho(x_i)$ gives (19). Now to solve the problem at time index $i + 1$ there are available two initial state conditions to solve (3). One is the prediction made at time index i for $i + 1$, \bar{x}_{i+1} from (19), and the other one is defined by the state measurements at $i + 1$, x_{i+1} from (2). This leads to two MPC problems we denote here by $\mathcal{P}_\rho(\bar{x}_{i+1})$ and $\mathcal{P}_\rho(x_{i+1})$, respectively. Note that both problems are solved with the same model, and the difference between their solutions reflects the degree of plant/model mismatch – Figure 1:

- $\mathcal{P}_\rho(\bar{x}_{i+1})$ – using ρ and \bar{x}_{i+1} , we obtain:

$$\Upsilon^*(\bar{x}_{i+1}) = \sum_{k=i+1}^{i+p} h(\bar{x}_k^*, \bar{u}_k^*) + \underbrace{h(\bar{x}_{i+p+1}^*)}_{=0} + P(\bar{\mathbf{s}}_{i+1}^*, \rho). \quad (22)$$

From the perfect model case we assume that ρ is large enough in order to obtain feasible solutions to $\mathcal{P}(\bar{x}_{i+1})$ if they exist. Thus the arguments for the perfect model case are also valid for this case.

- $\mathcal{P}_\rho(x_{i+1})$ – using ρ and x_{i+1} , we obtain:

$$\Upsilon^*(x_{i+1}) = \sum_{k=i+1}^{i+p} h(x_k^*, u_k^*) + \underbrace{h(x_{i+p+1}^*)}_{=0}$$

$$+ P(\mathbf{s}_{i+1}^*, \rho) = \sum_{k=i+1}^{i+p+1} h(x_k^*, u_k^*, \rho). \quad (23)$$

Since x_{i+1} can be different from \bar{x}_{i+1} , we may not have $P(\mathbf{s}_{i+1}^*, \rho) = 0$.

3.2.1. Sufficient condition for robust stability

To account for the existence of mismatch we consider the addition and subtraction of $\Upsilon^*(\bar{x}_{i+1})$ to the difference $\Upsilon^*(x_i) - \Upsilon^*(x_{i+1})$,

$$\begin{aligned} \Upsilon^*(x_i) - \Upsilon^*(x_{i+1}) &= \Upsilon^*(x_i) - \Upsilon^*(\bar{x}_{i+1}) \\ &\quad - (\Upsilon^*(x_{i+1}) - \Upsilon^*(\bar{x}_{i+1})). \end{aligned} \quad (24)$$

The term $\Upsilon^*(x_i) - \Upsilon^*(\bar{x}_{i+1})$ represents the difference between the optimal objective functions as in (20). Thus it follows that

$$\begin{aligned} \Upsilon^*(x_i) - \Upsilon^*(x_{i+1}) &\geq \\ h(x_i, u_i^*, \rho) &- (\Upsilon^*(x_{i+1}) - \Upsilon^*(\bar{x}_{i+1})). \end{aligned} \quad (25)$$

To ensure a closed loop stable system, we force the right hand side to be bounded by a positive function $W(\|x_i\|)$ of class \mathcal{K}_∞ . This ensures that the sequence $\{\Upsilon^*(x_i)\}$ is decreasing, that is,

$$h(x_i, u_i^*, \rho) - (\Upsilon^*(x_{i+1}) - \Upsilon^*(\bar{x}_{i+1})) \geq W(\|x_i\|), \quad (26)$$

with $W(\|x_i\|) \rightarrow 0$ as $\|x_i\| \rightarrow 0$, for all i , $i \geq 0$. The difference $\Upsilon^*(x_{i+1}) - \Upsilon^*(\bar{x}_{i+1})$ is a measure of the plant/model mismatch and henceforth we will refer to it as the *mismatch term*.

4. THE MISMATCH TERM

To characterize the mismatch term we start by invoking the mean value theorem to derive an expression for the mismatch term as a function of the difference between the two problem solutions. Then we consider the optimality conditions of both problems to derive a bound on the mismatch term, which leads to a sufficient condition for closed loop stability under the presence of plant/model mismatch.

4.1 Preliminaries

First of all, we assume that a value of ρ can be chosen that is sufficiently large. By invoking the mean value theorem it follows that

$$\begin{aligned} \Upsilon^*(x_{i+1}) - \Upsilon^*(\bar{x}_{i+1}) &= \\ \int_0^1 \left\{ \frac{d}{dx_{i+1}} \left[\Upsilon^*(\bar{x}_{i+1} + \tau(x_{i+1} - \bar{x}_{i+1})) \right]^T \right\} & \\ \cdot (x_{i+1} - \bar{x}_{i+1}) d\tau. \end{aligned} \quad (27)$$

This is done assuming (15) is differentiable. However, because of the exact penalty terms it is not. To overcome this we apply a smoothing

function (Balakrishna and Biegler, 1992) to every element of (16); e.g., for a scalar x ,

$$\max\{0, b(x)\} \approx b(x, \xi) = \frac{(b(x)^2 + \xi^2)^{1/2}}{2} + \frac{b(x)}{2} \quad (28)$$

with small $\xi > 0$. Henceforth (15) is replaced by

$$\Upsilon(x_i, \mathbf{s}_i, \rho_i, \xi) = \Psi(x_i, \mathbf{s}_i) + P(\mathbf{s}_i, \rho_i, \xi), \quad (29)$$

which is continuous and at least twice differentiable with respect to (6). For the forthcoming developments it is convenient to keep notation (18), and to define $k = 1, \dots, p$:

$$\varepsilon_{i+k}^* = [s_{i+k}^* - \bar{s}_{i+k}^*] = \begin{bmatrix} x_{i+k}^* - \bar{x}_{i+k}^* \\ u_{i+k}^* - \bar{u}_{i+k}^* \end{bmatrix}. \quad (30)$$

From (5), (28), (29) and (30), (27) becomes

$$\begin{aligned} \Upsilon^*(x_{i+1}) - \Upsilon^*(\bar{x}_{i+1}) &= \\ \sum_{k=1}^p \int_0^1 \nabla_{\mathbf{s}_{i+k}} h(\bar{\mathbf{s}}_{i+k}^* + \tau \varepsilon_{i+k}^*, \rho, \xi)^T \varepsilon_{i+k}^* d\tau. \end{aligned}$$

4.2 Derivation of a bound on the mismatch term

We start by considering the optimality conditions of problem $\mathcal{P}_\rho(x_{i+1})$. The Lagrangian for this problem is $\mathcal{L}(\mathbf{s}_{i+1}, \lambda) = \Upsilon(x_{i+1}) + \lambda^T \mathbf{c}(x_{i+1}, \mathbf{s}_{i+1})$, where λ is the Lagrange multiplier vector. The optimality conditions are:

$$\begin{bmatrix} \nabla_{\mathbf{s}} \Upsilon^*(x_{i+1}) + \nabla_{\mathbf{s}} \mathbf{c}(x_{i+1}, \mathbf{s}_{i+1}^*)^T \lambda^* \\ \mathbf{c}(x_{i+1}, \mathbf{s}_{i+1}^*) \end{bmatrix} = 0. \quad (31)$$

We also assume that $\nabla_{\mathbf{s}} \mathbf{c}(x_{i+1}, \mathbf{s}_{i+1}^*)$ has full row rank and we define a basis, Z , for the null space of this matrix, i.e., $\nabla_{\mathbf{s}} \mathbf{c}(x_{i+1}, \mathbf{s}_{i+1}^*) \cdot Z = 0$. By taking the projection of $\nabla_{\mathbf{s}} \Upsilon^*(x_{i+1}) + \nabla_{\mathbf{s}} \mathbf{c}(x_{i+1}, \mathbf{s}_{i+1}^*)^T \lambda^*$ on the null space of $\nabla_{\mathbf{s}} \mathbf{c}(x_{i+1}, \mathbf{s}_{i+1}^*)$, (31) becomes

$$\begin{bmatrix} Z^T \cdot \nabla_{\mathbf{s}} \Upsilon^*(x_{i+1}) \\ \mathbf{c}(x_{i+1}, \mathbf{s}_{i+1}^*) \end{bmatrix} = 0. \quad (32)$$

Thus proceeding as in the unconstrained case study (Santos and Biegler, 1999) we derive a bound for stability on the mismatch term,

$$\begin{aligned} |\Upsilon^*(x_{i+1}) - \Upsilon^*(\bar{x}_{i+1})| &\leq \\ \sum_{k=1}^p \left\| \int_0^1 \nabla_{\mathbf{s}_{i+k}} h(\bar{\mathbf{s}}_{i+k}^* + \tau \varepsilon_{i+k}^*, \rho, \xi)^T d\tau \right\| & \\ \cdot \Gamma \cdot W_m(\|x_i\|), \end{aligned} \quad (33)$$

that provides a sufficient stability condition for a general cost function $h(x, u)$, where Γ is derived from sensitivity information from (32) (see Santos and Biegler (1999)).

4.3 Constrained MPC with quadratic function and finite horizon

Typically, in MPC formulations (5) is defined with

$$h(s_{i+k}) = s_{i+k}^T Q_{i+k} s_{i+k}, \quad (34)$$

where $Q_{i+k} = \text{diag}\{Q_{x_{i+k}}, Q_{u_{i+k}}\}$, and $Q_{x_{i+k}} \in \mathbf{R}^{n_s \times n_s}$ and $Q_{u_{i+k}} \in \mathbf{R}^{n_m \times n_m}$ are diagonal matrices corresponding to the state and input weighting matrices at predictive horizon time index $i+k$, respectively. From (34), the analytical form of the integral term in (33) is

$$\int_0^1 \nabla_{s_{i+k}} h(\bar{s}_{i+k}^* + \tau \varepsilon_{i+k}^*, \rho, \xi)^\top d\tau = (2\bar{s}_{i+k}^* + \varepsilon_{i+k}^*)^\top Q_{i+k} + \rho \cdot r(\bar{s}_{i+k}^*, \varepsilon_{i+k}^*, \xi), \quad (35)$$

where $r(\bar{s}_{i+k}^*, \varepsilon_{i+k}^*, \xi)$ denotes a vector whose elements are nonlinear functions of \bar{s}_{i+k}^* , ε_{i+k}^* and ξ . Following the same developments as in Santos and Biegler (1999) we obtain

$$\begin{aligned} |\Upsilon^*(x_{i+1}) - \Upsilon^*(\bar{x}_{i+1})| \leq & \sum_{k=1}^p \left\{ \left(\|2\bar{s}_{i+k}^*\| + \|\varepsilon_{i+k}^*\| \right) \|Q_{i+k}\| \right. \\ & \left. + \rho \cdot \left\| r(\bar{s}_{i+k}^*, \varepsilon_{i+k}^*, \xi) \right\| \right\} \cdot \Gamma \cdot W_m(\|x_i\|). \quad (36) \end{aligned}$$

We assume there are positive constants Q , α_1 and α_2 , such that for all $i \geq 0$ and $k \leq p$

$$\left\| r(\bar{s}_{i+k}^*, \varepsilon_{i+k}^*, \xi) \right\| \leq \alpha_1 \|2\bar{s}_{i+k}^*\| + \alpha_2 \|\varepsilon_{i+k}^*\| \quad (37)$$

and $\|Q_{i+k}\| \leq Q$. Moreover, since \bar{s}_{i+k}^* , $k = 1, \dots, p$, depends on x_i , we set

$$\|2\bar{s}_{i+k}^*\| \leq \hat{K} \|x_i\|, \quad (38)$$

where \hat{K} is a positive constant. From (4), with $\gamma = 1$ (see Santos and Biegler (1999)),

$$\|\varepsilon_{i+k}^*\| \leq \Gamma \cdot W_m(\|x_i\|) \leq \Gamma K_m \|x_i\|, \quad (39)$$

for every k , $k \leq p$. Finally, substituting (37), (38) and (39) in (36) leads to

$$|\Upsilon^*(x_{i+1}) - \Upsilon^*(\bar{x}_{i+1})| \leq K_B \|x_i\|^2, \quad (40)$$

where $K_B = p \left\{ (\hat{K} + \Gamma K_m) Q + \rho \cdot (\alpha_1 \hat{K} + \alpha_2 \Gamma K_m) \right\} \Gamma K_m$. (41)

Note that the first term of the sum on the right hand side of (41) is the expression of K_B obtained for the unconstrained case. Therefore, when there are no active constraints $\rho = 0$ and (40) is equal to the unconstrained case sufficient stability bound. Also, from (26) and (40) it follows that

$$\begin{aligned} h(x_i, u_i^*, \rho) - |\Upsilon^*(x_{i+1}) - \Upsilon^*(\bar{x}_{i+1})| \\ \geq h(x_i, u_i^*) - K_B \|x_i\|^2 = W(\|x_i\|). \quad (42) \end{aligned}$$

Suppose that $Q_{x_i} = \alpha_x I$ and $Q_{u_i} = \alpha_u I$, with constants $\alpha_x > 0$ and $\alpha_u \geq 0$. Because u_i^* is an implicit function of x_i we can write $\|u_i^*\|^2 = \beta \|x_i\|^2$, $\beta > 0$. Thus

$$h(x_i, u_i^*) = \alpha_x x_i^\top x_i + \alpha_u u_i^{*\top} u_i^* = (\alpha_x + \alpha_u \beta) \|x_i\|^2 \quad (43)$$

For a given x_i , with no active constraints, and with $\alpha_u = 0$, from (42) it follows that $K_B < \alpha_x$ to

satisfy the sufficient condition for stability. When $\alpha_u \neq 0$, this condition is relaxed to

$$K_B < \alpha_x + \alpha_u \beta. \quad (44)$$

4.4 A tool to analyze robust stability

Because β in (44) depends on the optimization problem solution it is impossible to know a priori K_B . In Section 5 we illustrate that $K_B < \alpha_x$ provides a conservative sufficient condition for stability. In any case, when constraint violations occur a tighter value of the sufficient stability condition for the constrained case, K_B , can be estimated by exploiting the state-space region of interest from

$$K_B \geq \max_{x_i} \frac{|\Upsilon^*(x_{i+1}) - \Upsilon^*(\bar{x}_{i+1})|}{\|x_i\|^2}. \quad (45)$$

This procedure involves the calculation off-line of K_B according to the following cycle:

- 1 For a given x_i , $i \geq 0$, perform the following steps:
- 2 Solve $\mathcal{P}_\rho(x_i)$; save \bar{x}_{i+1} .
- 3 Implement u_i^* and set $i = i + 1$.
 - i Using x_{i+1} , solve $\mathcal{P}_\rho(x_{i+1})$ to obtain $\Upsilon^*(x_{i+1})$.
 - ii Using \bar{x}_{i+1} , solve $\mathcal{P}_\rho(\bar{x}_{i+1})$ to obtain $\Upsilon^*(\bar{x}_{i+1})$.
 - iii Go to 1 and repeat steps with new values of x_i .

Therefore for a nonzero x_i we can compute a lower bound for K_B .

5. ILLUSTRATIVE EXAMPLE

Consider an exothermic zero-order reaction system, $A \rightarrow B$, with concentration and temperature dynamics described by

$$\frac{dC_A}{dt} = \frac{F_0}{V} (C_{A0} - C_A) - k_0 e^{-E_a/(R T_r)}, \quad (46)$$

$$\frac{dT_r}{dt} = \frac{1}{\rho_L C_p V} (-Q_R + Q_G), \quad (47)$$

with $Q_R = -\rho_L C_p F_0 (T_0 - T_r) + UA(T_r - T_j)$, and $Q_G = (-\Delta H_r) V k_0 e^{-E_a/(R T_r)}$. Note that (47) does not depend on C_A . The system is open loop unstable for $T_{r,i} > 34^\circ\text{C}$. Data and a more detailed description of this system can be found in Santos (2001). The control objective is to control T_r - the set-point is $T_{r,sp} = 34^\circ\text{C}$ - by manipulating the cooling fluid temperature T_j subject to: $T_r \geq 0^\circ\text{C}$ and $T_j \geq 15^\circ\text{C}$. To satisfy these constraints the control problems are solved using (15) with $\rho = 1000$. We set $(\alpha_x, \alpha_u) = (1, 0)$, $(p, m) = (25, 1)$, $\Delta t = 0.5 \text{ min}$ and we note that the plant and the model have the same steady state with $T_r = T_j = 34^\circ\text{C}$. To test for the sufficient stability condition parametric model mismatch on U is considered. Figure 2 shows the variation of K_B with $T_{r,i}$, varying from 24 to 44°C , and for various mismatches: $U_m =$

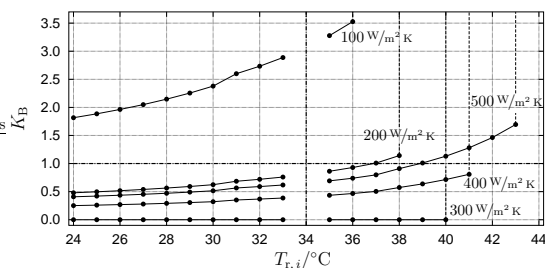


Fig. 2. Variation of the constant bound.

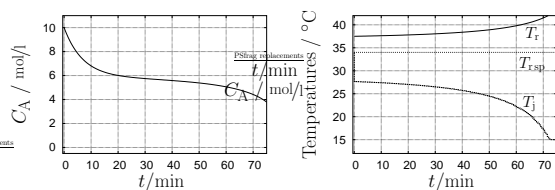


Fig. 3. Unstable regulator control response.

100, 200, 300, 400 and 500 $\text{W/m}^2\text{K}$. The true plant value is $U_p = 300 \text{ W/m}^2\text{K}$. Thus, we observe in Figure 2 that in the case of perfect model $K_B = 0$. We emphasize that when the constraints are not satisfied then (16) is not zero and K_B is very high. Here, the nonexistence of a feasible solution is overcome by increasing appropriately p to pursue the calculation of K_B .

For $(\alpha_x, \alpha_u) = (1, 0)$, a sufficient condition for robust stability from (42) requires $K_B < 1$. This can be seen in Figures 2 and 3. For $T_{r,i} < 34^\circ\text{C}$, the profiles show $K_B < 1$ always. Under these conditions the system is closed loop stable in the sense that the state converges to the origin (set-point), $T_r = 34^\circ\text{C}$. On the other hand, for $T_{r,i} > 34^\circ\text{C}$, the profiles of K_B increase such that they tend to cross the line $K_B = 1$ as $T_{r,i}$ increases. Since (45) provides a lower bound on K_B it means the system can become closed loop unstable under these plant/model mismatch conditions – e.g., Figure 3 with $T_{r,i} = 37.5^\circ\text{C}$ and $U_m = 400 \text{ W/m}^2\text{K}$. On the other hand, with $U_m = 500 \text{ W/m}^2\text{K}$, the system is closed loop unstable when $T_{r,i} > 34^\circ\text{C}$. Again, from (45) this is consistent with the theory since $K_B > 1$ for $T_{r,i} \geq 39^\circ\text{C}$.

On the other hand, stable performance may still be observed if (42) is violated because this condition is only sufficient. For instance, with $U_m = 100 \text{ W/m}^2\text{K}$ the system is closed loop stable despite $K_B > 1$. The same result is observed for $U_m = 200 \text{ W/m}^2\text{K}$ when $T_{r,i} \geq 37^\circ\text{C}$. In these cases $U_p > U_m$, thus the control solution is favorable to the plant; i.e., the control system provides a cooling rate greater than the one really necessary. But for $U_m = 400$ and $500 \text{ W/m}^2\text{K}$ the cooling rate calculated by the controller may not be sufficient to cool down the reactor liquid and therefore a temperature runaway may occur.

6. CONCLUSIONS

We develop a strategy based on nonlinear programming sensitivity that determines conditions under which the constrained model predictive control is robustly stable with respect to modeling errors. Here, a sufficient condition for robust stability is derived and an offline procedure is developed to evaluate constants which determine sufficient conditions for this property. These constants are available from bounds on the model mismatch and from the NLP solution of the receding horizon model. This procedure is applicable to both linear and nonlinear model predictive controllers in discrete time that satisfy nominal stability properties based on Lyapunov arguments.

ACKNOWLEDGEMENTS

L.O.S. is grateful for financial support provided by *Fundação para a Ciência e Tecnologia* under grant PRAXIS XXI/BD/2757/94.

7. REFERENCES

- Balakrishna, S. and L. T. Biegler (1992). Targeting Strategies for the Synthesis and Energy Integration of Nonisothermal Reactor Networks. *Ind. Eng. Chem. Res.* **31**, 2152–2164.
- Fletcher, R. (1987). *Practical Methods of Optimization*. second ed.. John Wiley & Sons Ltd.. Chichester.
- Keerthi, S. S. and E. G. Gilbert (1988). Optimal Infinite-Horizon Feedback Laws for General Class of Constrained Discrete-Time Systems: Stability and Moving-Horizon Approximations. *IEEE Trans. Auto. Cont.* **57**(2), 265–293.
- Mayne, D. Q., J. B. Rawlings, C. V. Rao and P. O. M. Sokaert (2000). Constrained Model Predictive Control: Optimality and stability. *Automatica* **36**(6), 789–814.
- Oliveira, N. M. C and L. T. Biegler (1994). Constraint Handling and Stability Properties of Model Predictive Control. *AIChE J.* **40**(7), 1138–1155.
- Santos, L. O. (2001). Multivariable Predictive Control of Chemical Processes. PhD thesis. Faculdade de Ciências e Tecnologia, Universidade de Coimbra. Coimbra, Portugal.
- Santos, L. O. and L. T. Biegler (1999). A Tool to Analyze Robust Stability for Model Predictive Controllers. *Journal of Process Control* **9**, 233–246.
- Santos, L. O., N. M. C. Oliveira and L. T. Biegler (1995). Reliable and Efficient Optimization Strategies for Nonlinear Model Predictive Control. In: *Proc. of DYCORD+ '95, Helsingør, Denmark* (J. B. Rawlings, Ed.). Elsevier Science. Oxford. pp. 33–38.

RELATIONSHIP BETWEEN CONTROL-RELEVANT NONLINEARITY AND PERFORMANCE OBJECTIVE

Nicholas Hernjak* Francis J. Doyle III**,¹
Frank Allgöwer*** Tobias Schweickhardt***

* *Department of Chemical Engineering, University of Delaware,
Newark, DE, USA*

** *Department of Chemical Engineering, University of California,
Santa Barbara, CA, USA*

*** *Institut für Systemtheorie Technischer Prozesse, Universität
Stuttgart, Stuttgart, Germany*

Abstract: In this work, the relationship between performance objective and control-relevant nonlinearity was investigated for Hammerstein and Wiener systems with polynomial nonlinearities. Nonlinearity assessment of the systems' inverses augmented with first-order linear filters using a numerical measure of nonlinearity showed that the nonlinearity varies depending on the relative magnitude of the filter time constant, but generally showed increasing nonlinearity with decrease in time constant. Similar assessment of the respective nonlinear internal model control structures indicated that the Hammerstein nonlinearity is weakly dependent on the filter time constant while the Wiener nonlinearity is strongly dependent.

Keywords: Nonlinear control systems, Nonlinear models, Performance analysis, Optimal control, Inverse system

1. INTRODUCTION

A key step in designing a control strategy for a process is determining the degree of complexity of the control algorithm necessary to optimally compensate for the intrinsic process nonlinearity (Ogunnaike *et al.*, 1993). As demonstrated previously (Hernjak *et al.*, 2002), certain nonlinear behaviors are more severe than others and some that appear significant in the open-loop setting may have little impact on closed-loop behavior.

Work involving use of the optimal control structure (OCS) as a means for assessing control-relevant nonlinearity (Stack and Doyle III, 1997) emphasized another issue of importance in deter-

mining the optimal degree of controller nonlinearity: the cost of the control action, or similarly, the desired level of performance of the controller. The implication of these results is that it is not only the inherent nonlinearity of the process that is of importance, but also the desired level of performance of the controller. In this work, a numerical measure of nonlinearity is employed to characterize the relationship between degree of controller nonlinearity and its performance objective for Hammerstein and Wiener systems with polynomial nonlinearities and scalar dynamics.

The particular control structures characterized in this work are nonlinear internal model control (IMC) algorithms. IMC algorithms involve the use of an explicit model of the process in order to compensate for uncertainty, including unmeasured disturbances (Morari and Zafiriou, 1989). Control

¹ Author to whom correspondence should be addressed.
E-mail: doyle@engineering.ucsb.edu

actions are generated from the disturbance prediction using an inverse of the model augmented with a unity-gain filter to maintain realizability. The filter time constant is introduced as a tuning parameter to adjust controller aggressiveness. Analysis of this type was suggested previously (Stack and Doyle III, 1999) using coherence as the measure of nonlinearity. Use of strictly linear IMC algorithms in determining the applicability of linear feedback for a process has also been investigated (Eker and Nikolaou, 2002). Other methods for analyzing control-relevant nonlinearity have also been proposed (Guay *et al.*, 1995).

In Section 2, the nonlinearity measure is introduced. In Section 3, the open-loop nonlinearity of the Hammerstein and Wiener structures is discussed. In Section 4, the nonlinearity of the model inverse plus filter is investigated. Finally, in Section 5, the nonlinearity of the classical IMC structure is analyzed.

2. NONLINEARITY MEASURE

The numerical nonlinearity measure proposed originally in (Allgöwer, 1995) and elaborated upon in (Helbig *et al.*, 2000) was used for nonlinearity characterization:

$$\phi_N^{\mathcal{U}} = \inf_{G \in \mathcal{G}} \sup_{\mathbf{u} \in \mathcal{U}} \frac{\|G[\mathbf{u}] - N[\mathbf{u}]\|_{\mathcal{P}\mathcal{Y}}}{\|N[\mathbf{u}]\|_{\mathcal{P}\mathcal{Y}}} \quad (1)$$

where $N : \mathcal{U} \rightarrow \mathcal{Y}$ is the system operator and $G : \mathcal{U} \rightarrow \mathcal{Y}$ is a linear approximation to N . \mathcal{U} is the space of considered input signals, \mathcal{Y} is the space of admissible output signals, and \mathcal{G} is the space of linear operators. $\phi_N^{\mathcal{U}}$ is a number between zero and one where a value of zero indicates the existence of a linear approximation to the system whose output matches the output of the original system over the set of inputs being considered. A value close to one indicates a highly nonlinear system.

As (1) represents an infinite dimensional optimization problem, approximate computational techniques are utilized to compute lower bounds on the measure. A general computational technique involves selecting a representative set of inputs and then building a linear approximation composed of a weighted sum of linear basis functions, e.g.:

$$y(s) = w_o u(s) + \sum_{i=1}^{N_l} \frac{w_i}{\tau_i s + 1} u(s) \quad (2)$$

w_i are the weights on the basis functions, τ_i are the functions' time constants, and N_l is the number of basis functions chosen. It has been shown (Allgöwer, 1995) that the search for the

optimal set of w_i is convex. In this work, a quasi-Newton optimization algorithm with numerical Hessian update was employed to calculate the w_i .

A less rigorous but more computationally efficient lower bound on (1) can be obtained by limiting the space of admissible inputs to sinusoids of varying amplitude and frequency. Provided that the nonlinear system preserves periodicity, the output after any transients have decayed can be represented by a Fourier series:

$$y_s = A_o + \sum_{k=1}^{\infty} A_k \cdot \sin(k\omega t + \phi_k) \quad (3)$$

By choosing the norm:

$$\|y(t)\| = \lim_{T \rightarrow \infty} \sqrt{\frac{1}{T} \int_0^T y^2(t) dt} \quad (4)$$

it can be shown (Allgöwer, 1995) that the following is a lower bound on (1):

$$\chi_N^{\mathcal{U}_s} = \sup_{a \in \mathcal{A}, \omega \in \Omega} \sqrt{1 - \frac{A_1^2}{2A_o^2 + \sum_{k=1}^{\infty} A_k^2}} \quad (5)$$

where \mathcal{A}, Ω are the sets of input signal amplitudes and frequencies being considered. $\chi_N^{\mathcal{U}_s}$ usually lies within 10-15% of the best value obtained through use of the optimization method discussed above.

3. OPEN-LOOP NONLINEARITY

The Hammerstein and Wiener models studied in this work consist of a first-order linear dynamic element with unity gain and time constant and a static polynomial nonlinearity of order n . The Hammerstein model is of the form:

$$v = u^n, \quad \dot{x} = -x + v, \quad y = x \quad (6)$$

and the Wiener model is of the form:

$$v = u, \quad \dot{x} = -x + v, \quad y = x^n \quad (7)$$

Hammerstein and Wiener model structures have been applied in modeling many nonlinear process systems (e.g., (Eskinat *et al.*, 1991), (Pottman and Pearson, 1996)) including pH systems and systems with nonlinear control valves.

The degree of open-loop nonlinearity for these systems is assessed using the LB (5). An input range of $0 \leq u(t) \leq 1$ centered at a steady-state of $u = 0.5$ is considered along with integer values of n ranging from 2 to 5. It is informative to consider the value of (5) computed at each frequency individually to study how different frequencies contribute to the nonlinearity measure,

as is plotted in Figures 1 and 2. This will be referred to as the frequency dependence of (5), but note that the true value of (5) is the maximum value of each of the curves. The results show that the frequency dependence of (5) follows opposite trends for the two systems with the Wiener system reaching its highest values at low frequency and the Hammerstein system approaching its highest values at high frequency. The results also indicate a trend of increasing nonlinearity with n .

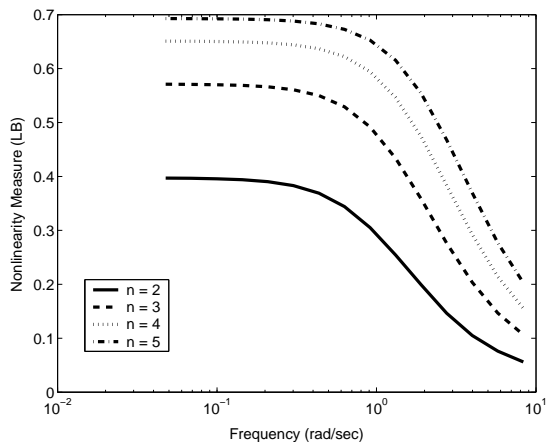


Fig. 1. Frequency dependence of Wiener system open-loop nonlinearity as measured using the LB (5) for various polynomial orders and an operating range of $0 \leq u(t) \leq 1$.

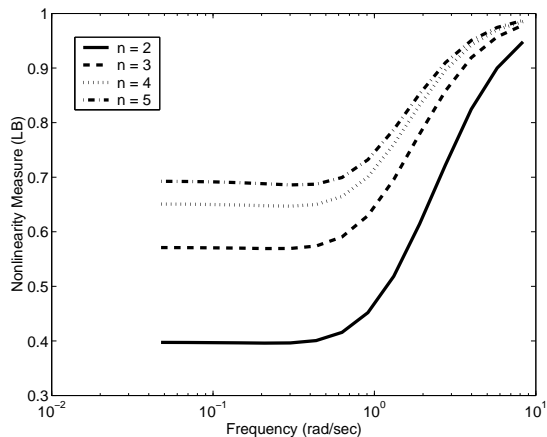


Fig. 2. Frequency dependence of Hammerstein system open-loop nonlinearity as measured using the LB (5) for various polynomial orders and an operating range of $0 \leq u(t) \leq 1$.

An analysis of the results in Figures 1 and 2 reveals that the low frequency results are identical for both systems. Because the low frequencies correspond to the region below the reciprocal time constant (1 rad/sec), these results correspond to the steady-state nonlinearity of the system, thus negating any effects of the linear dynamics and its placement in the structure.

The high frequency behavior is explainable by considering the frequency behavior of the linear

dynamics. The linear dynamics are first order and therefore attenuate to an increasing degree the higher frequency inputs. As can be seen in Figure 3, for the Wiener system at high frequencies, the linear dynamics attenuate the single-frequency input to the point where the nonlinearity has little effect.

For the Hammerstein system, the static nonlinearity will first generate additional frequencies due to the ability of many nonlinear functions to generate harmonics (Pearson, 1999). The result of this, as can be seen in Figure 3, is that the final output exhibits a large positive bias from the steady-state value due to the linear dynamics not attenuating the zero-frequency harmonic (steady-state bias) generated by the static nonlinearity. This bias adds greatly to the value of the nonlinearity measure.

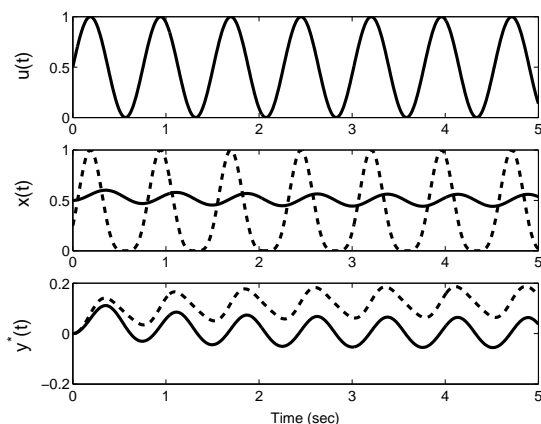


Fig. 3. Wiener (solid) and Hammerstein (dashed) systems time-domain signals for an input sinusoid of amplitude 0.5 and frequency 8.33 rad/sec when $n = 2$. $y^*(t)$ is the deviation from the steady-state output.

The results provided in this section are generalizable to other static nonlinearities and linear dynamics with only slight modifications as they rely only on the generation of harmonics by a nonlinear system and the attenuation characteristics of the dynamics.

4. SYSTEM INVERSE NONLINEARITY

In the linear IMC framework, its ISE optimal control results from the use of specific filters (which depend on input characteristics) coupled with the appropriate model inverse. While the optimality properties do not transfer directly to nonlinear IMC structures, these structures are still important for control-relevant analysis since they maintain many of the useful qualities of linear IMC structures (Economou *et al.*, 1986). The equivalent classical controller designs arising from IMC algorithms for the Hammerstein and

Wiener systems are shown in Figures 4 and 5. As outlined in the figures, the nonlinearity of the individual elements of these control structures and the overall structures themselves are considered separately in the sections of this paper. In this section, the nonlinearity of just the process inverse is considered as this structure corresponds to the IMC algorithm in the ideal case when there is no model error or output disturbances. In that case, the process inverse serves as an open-loop controller relating setpoint changes to manipulated variable moves.

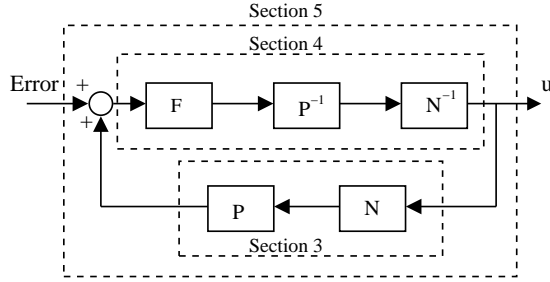


Fig. 4. Classical control structure corresponding to IMC design for a Hammerstein system. P = linear dynamics, N = static nonlinearity, F = filter.

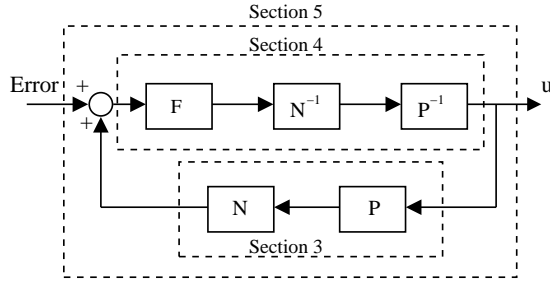


Fig. 5. Classical control structure corresponding to IMC design for a Wiener system. P = linear dynamics, N = static nonlinearity, F = filter.

To ensure realizability, the inverse is augmented with a first-order filter:

$$F(s) = \frac{1}{\lambda s + 1} \quad (8)$$

where λ is the filter time constant. A first-order design is the minimum filter order necessary in this case to maintain realizability. Higher order filters could be designed but would correspond to controller designs with sluggish dynamic properties.

As seen in Figure 4 (Hammerstein structure), the inverse of the linear dynamics for a first-order system augmented with the filter is a lead-lag system, i.e.:

$$FP^{-1}(s) = \frac{s + 1}{\lambda s + 1} \quad (9)$$

Therefore, the frequency behavior of the system is a function of the filter time constant. For large λ , the lag behavior of the system dominates and the high-frequency signals are attenuated, while for small λ , the lead behavior dominates and the high-frequency signals are magnified. Similar observations can be made for the Wiener system, but note that the filter and the inverse linear dynamics are separated by the inverse of the static nonlinearity. The nonlinearity of the inverse systems is considered in the range $0 \leq y(t) \leq 1$ centered at $y = 0.5$.

The effects of the lead-lag element on the nonlinearity can be seen for the Hammerstein system in Figure 6. At large λ values, the lag behavior dominates and the nonlinearity follows the Wiener trend seen in Figure 2. At small λ , the lead behavior dominates and there exists a maximum nonlinearity in the middle of the frequency range. It should be noted that, at low frequency, all of the curves in Figure 6 asymptote to the nonlinearity of the static nonlinearity block. Figure 7 is the corresponding plot for the Wiener inverse, demonstrating the same trend as the open-loop Wiener system for large λ and a completely different trend for low λ . The large λ trend is expected as the filter placement causes the first two blocks of the inverse to resemble a Wiener system of their own with a time constant that will dominate that of the inverse linear dynamics. Note that, for the Wiener system, the $\lambda = 1$ trend is not flat thus showing the effect of placing the nonlinearity between the two linear dynamic blocks.

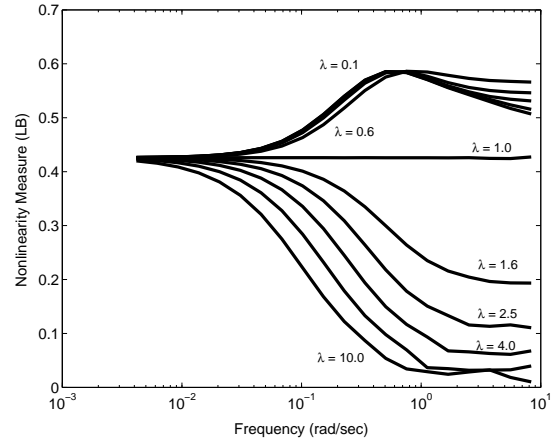


Fig. 6. Inverse Hammerstein system ($n = 3$) nonlinearity as a function of frequency for various values of the filter time constant, λ .

By the definition of (5), the true nonlinearity of the inverse system is the maximum value over the frequency range for each value of λ . Figure 8 shows these results for both systems. For the Hammerstein system, the inverse's nonlinearity is a weak function of λ over selected intervals. For $\lambda \geq 1$, the nonlinearity is that of the static nonlinearity block and for $\lambda < 1$, the nonlinearity

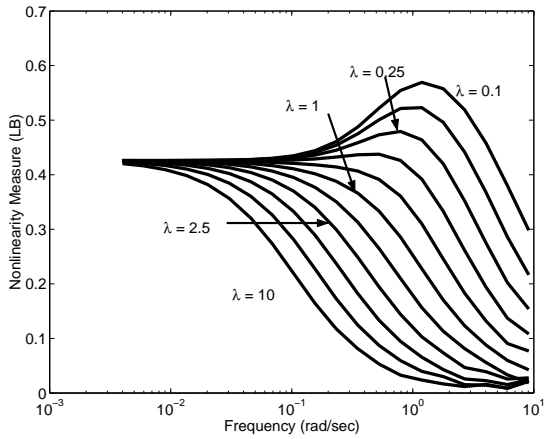


Fig. 7. Inverse Wiener system ($n = 3$) nonlinearity as a function of frequency for various values of the filter time constant, λ .

is that of the peak value shown in Figure 6. For the Wiener inverse, the nonlinearity matches that of the Hammerstein system for $\lambda > 1$ and steadily grows for $\lambda < 1$.

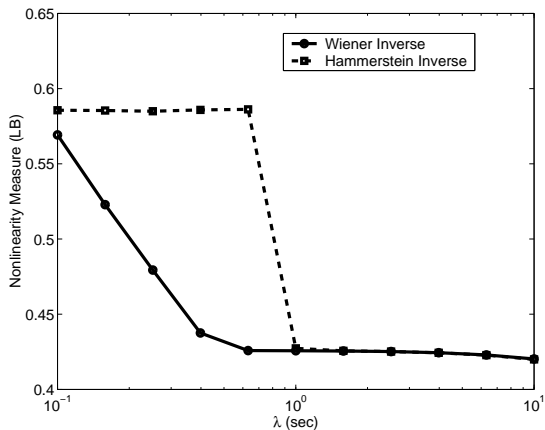


Fig. 8. Wiener and Hammerstein systems ($n = 3$) inverse nonlinearity as a function of the filter time constant, λ .

The conclusion that can be drawn from the data presented in this section is that the nonlinearity of these system inverses is dictated by the time constant of the linear filter (i.e., the closed-loop time constant). As the filter time constant varies in magnitude relative to the system’s open-loop time constant, the severity of the nonlinearity changes in differing manners. Admittedly, consideration of λ values greater than one is not of much practical relevance since such tunings would correspond to a closed-loop time constant that is larger than the open-loop time constant. It is informative to consider the $\lambda > 1$ case since the overall results indicate a trend of increasing nonlinearity as one proceeds from the $\lambda > 1$ region to the $\lambda < 1$ region, corresponding to an increase in desired controller performance.

5. CLASSICAL CONTROL STRUCTURE NONLINEARITY

The final step in the control analysis is to consider the classical realization of the IMC controller. As shown in Figures 4 and 5, the input considered now is the setpoint error ($y_d - y$, where y_d is the set-point). This form of the IMC design is referred to as the “classical” realization, equivalent to the form of PID and other standard control algorithms in which setpoint error is the input and manipulated variable value is the output.

As is desired for this realization, the controllers will integrate the input (error) signals. For instance, for the Hammerstein structure, the N^{-1} block can be moved beyond the loop leaving a purely linear loop. In that case, it can be shown that the equivalent loop operator has the form:

$$L(s) = \frac{s + 1}{\lambda s} \quad (10)$$

containing integral action. For the Wiener case, the P^{-1} block can be moved beyond the loop first followed by the N^{-1} block leaving only the filter in the feedback loop. The loop operator thus reduces to $1/\lambda s$, again showing integral action. The preceding analysis also demonstrates that the classical structures have the same general structures as the process inverses, i.e., the Hammerstein controller has a Wiener structure and the Wiener controller has a “linear-nonlinear-linear” block sandwich structure.

Given the integrating nature of the systems, the LB formulation of the nonlinearity measure cannot be used. Instead, the optimization-based algorithm discussed in Section 2 was used to characterize the system nonlinearity for a finite time horizon. Twenty stochastic input signals were implemented spanning the same magnitude and frequency ranges of $u(t)$ used to characterize the inverse system nonlinearity. The basis functions chosen for the linear approximation included one pure integrator and two unstable functions (i.e., $\tau_i < 0$) to account for any other positive feedback-induced behaviors of the system as well as 13 stable first-order lags with logarithmically-spaced $\tau_i \in [0.075, 60]$.

Figure 9 includes the results of the classical IMC nonlinearity assessment. The slight roughness of the trends in Figure 9 is due to the stochastic nature of the input signals. Signals with more precisely designed frequency content would result in smoother trends.

The Hammerstein system nonlinearity in Figure 9 is essentially invariant with respect to λ , which is consistent with the results for the inverse nonlinearity in Figure 8. The result in this case is due to the role of λ in the loop operator (10) in which

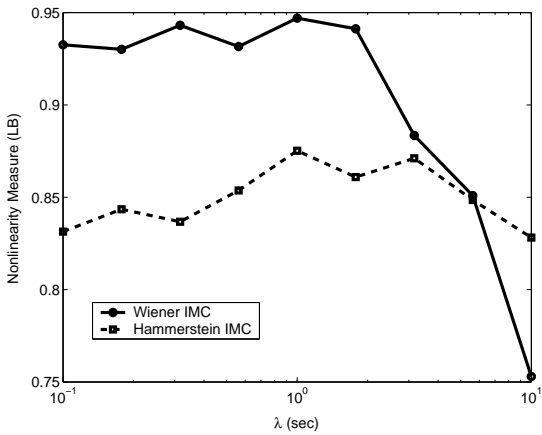


Fig. 9. Nonlinearity of the classical IMC structures as functions of the filter tuning parameter, λ .

it acts purely as a gain, therefore affecting all frequency components uniformly. For the Wiener system, the results in Figure 9 suggest a uniformly high nonlinearity for the $\lambda < 1$ region and a sharp decrease beyond $\lambda = 1$ again indicating decreased nonlinearity with detuning. In general, the results indicate that the nonlinearity of the controller necessary to effectively control either of these systems is quite high.

6. CONCLUSIONS

The results of this work demonstrate that the performance objective of a controller can greatly impact the control-relevant nonlinearity of the system. It was shown that the degree of nonlinearity of the process inverses and the classic realizations of the IMC controller is strongly dependent on the relative magnitude of the filter time constant as compared to the open-loop time constant for Wiener systems and, at most, weakly dependent for Hammerstein systems.

The results in Section 3 showed that the open-loop nonlinearity of the Hammerstein systems is generally greater than that of the Wiener systems. In comparing these results to the control-relevant results, it is suggested that the high Hammerstein open-loop nonlinearity mandates a uniformly high controller nonlinearity to optimally control these systems. For the Wiener systems, highly nonlinear control is only necessary when high levels of performance are desired. Therefore, at least in regards to IMC design, these common classes of systems are representative of two different cases:

- (1) highly nonlinear open-loop systems that require highly nonlinear control for optimal performance (Hammerstein),
- (2) mildly nonlinear open-loop systems that require highly nonlinear control *only* when high levels of performance are required (Wiener).

7. ACKNOWLEDGMENTS

Authors Hernjak and Doyle would like to acknowledge the Institut für Systemtheorie Technischer Prozesse at Universität Stuttgart for hosting them during the time when this work was formulated. Prof. Doyle would like to further acknowledge the Alexander von Humboldt Foundation for sabbatical fellowship support.

8. REFERENCES

- Allgöwer, F. (1995). Definition and computation of a nonlinearity measure. In: *3rd IFAC Nonlinear Control Systems Design Symposium*. Lake Tahoe, CA. pp. 279–284.
- Economou, C. G., M. Morari and B. O. Palsson (1986). Internal model control. 5. Extension to nonlinear systems. *Ind. Eng. Chem., Process Des. Dev.* **25**, 403–411.
- Eker, S. A. and M. Nikolaou (2002). Linear control of nonlinear systems - the interplay between nonlinearity and feedback. *AIChE J.* **48**(9), 1957–1980.
- Eskinat, E., S. H. Johnson and W. L. Luyben (1991). Use of Hammerstein models in identification of nonlinear systems. *AIChE J.* **37**(2), 255–268.
- Guay, M., P.J. McLellan and D.W. Bacon (1995). Measurement of nonlinearity in chemical process control systems: The steady state map. *Can. J. Chem. Eng.* **73**, 868–882.
- Helbig, A., W. Marquardt and F. Allgöwer (2000). Nonlinearity measures: Definition, computation and applications. *J. Process Contr.* **10**, 113–123.
- Hernjak, N., F. J. Doyle III and R. K. Pearson (2002). Control-relevant characterization of nonlinear classes of process systems. In: *Proc. IFAC World Congress*. Barcelona.
- Morari, M. and E. Zafiriou (1989). *Robust Process Control*. Prentice-Hall, Englewood Cliffs, NJ.
- Ogunnaike, B. A., R. K. Pearson and F. J. Doyle III (1993). Chemical process characterization: With applications in the rational selection of control strategies. In: *Proceedings of the European Control Conference*. Groningen, The Netherlands. pp. 1067–1071.
- Pearson, R. K. (1999). *Discrete-Time Dynamic Models*. Oxford University Press. New York.
- Pottman, M. and R.K. Pearson (1996). Gray-box modelling of processes with output multiplicities. In: *IFAC World Congress*. San Francisco, USA. pp. 67–72.
- Stack, A. J. and F. J. Doyle III (1997). Application of a control-law nonlinearity measure to a chemical reactor. *AIChE J.* **43**, 425–447.
- Stack, A. J. and F. J. Doyle III (1999). Local nonlinear performance assessment for single controller design. In: *Proc. IFAC World Congress*. Beijing. pp. 111–117.

EFFECT OF PROCESS NONLINEARITY ON LINEAR QUADRATIC REGULATOR PERFORMANCE ¹

R. Dier * M. Guay ^{*,2} P.J. McLellan *

** Department of Chemical Engineering, Queen's University,
Kingston, Ontario, Canada K7L 3N6*

Abstract: In this paper, a new local measure of linear controller performance is introduced for linear controllers operating on a nonlinear plant. The measure, called the performance sensitivity measure, quantifies the departures from optimality of a locally linear quadratic regulators. The measure applies to nonlinear systems that admit a controllable and observable linearization. It is shown that the measure can be related to standard minimum variance benchmarking techniques and can therefore be assessed using closed-loop process data in an operating region of interest.

Keywords: Nonlinearity, Linear controller performance, Performance benchmarking

1. INTRODUCTION

The control of linear systems has been extensively studied and the literature provides a very complete and well-characterized collection of tools for their analysis, monitoring, optimization, and control. As a result, process control engineers focus on linear system representations to solve a wide range of control problems. Unfortunately, the reality is that few processes are linear, and therefore the effectiveness of using linear control strategies can be questioned. Nonlinear control strategies have advanced greatly, and are becoming more widely accepted; however, their implementation is impeded by a considerable degree of mathematical sophistication or computational

requirement. As a result local linear approximations of the nonlinear system are often used to develop a control law. In order to test the effectiveness of this approach, it would desirable to develop an index that measures the effect of process nonlinearity on linear controller performance. From a design point of view, such a measure would indicate whether sufficient benefit is available to warrant investment in a nonlinear controller.

Many authors (e.g., (Desoer and Wang 1981), (Allgöwer 1995a), (Allgöwer 1995b), (Stack and Doyle III 1997), (Haber 1985), (Ogunnaik *et al.* 1993), (Guay *et al.* 1995)) have considered the assessment of process nonlinearity as means of justifying the need for nonlinear control techniques. However such measures provide admittedly open-loop assessment of nonlinearity that are difficult to relate to controller performance. The objec-

¹ Work supported by the Natural Sciences and Engineering Council of Canada and the Canadian Foundation for Innovation

² To whom correspondence should be addressed.

tive of this paper is to introduce a new local measure of linear controller performance for linear controllers operating on a nonlinear plant. The measure, called the performance sensitivity measure, quantifies the departures from optimality of a locally linear quadratic regulators. The measure applies to nonlinear systems that admit a controllable and observable linearization. It is shown that the measure can be related to standard minimum variance benchmarking techniques and can therefore be assessed using closed-loop process data in an operating region of interest. The paper is structured as follows. The proposed performance sensitivity measure is presented in Section 2. In Section 3, we draw a parallel between the proposed measure and standard minimum variance benchmarking techniques. This is followed by brief conclusions in Section 6.

2. PERFORMANCE SENSITIVITY MEASURE

In this section, an alternative control-relevant nonlinearity measure, the “performance sensitivity measure”, is introduced. The performance sensitivity measure (PSM) attempts to characterize the extent of performance degradation expected when a nonlinear system is regulated by a linear quadratic regulator (LQR).

Consider the nonlinear time-invariant system,

$$\begin{aligned}\dot{x} &= f(x, u(t)) \\ y &= h(x(t))\end{aligned}\quad (1)$$

$u(t) \in \mathbb{R}^p$ is the available control input, $y(t) \in \mathbb{R}^m$ is the observed process output, and $x(t) \in \mathbb{R}^n$ represents the internal states of the system. The linearization of the system eq.(1) about the origin is given by the linear time-invariant system

$$\begin{aligned}\dot{x} &= Ax(t) + Bu(t) \\ y(t) &= Cx(t)\end{aligned}\quad (2)$$

where A , B , and C are system matrices of appropriate dimension. It is assumed that the triple (A, B, C) is both observable and controllable. By letting C be the identity matrix, full state information is available for use in the control strategy.

For the linear system eq.(2), the linear quadratic regulator given by

$$u(t) = -R^{-1}B^T Px(t) \quad (3)$$

minimizes, for every initial condition $x(0) = x_0$, the quadratic objective function,

$$\eta = \int_0^\infty (x^T(t)Qx(t) + u^T(t)Ru(t)) dt \quad (4)$$

where $Q \in \mathbb{R}^{n \times n}$ and $R \in \mathbb{R}^{p \times p}$ are problem-specific, non-negative definite state- and input-penalty matrices, and where P is the positive-definite, symmetric solution matrix of the algebraic Riccati equation

$$A^T P + PA - PBR^{-1}B^T P + C^T QC = 0 \quad (5)$$

The cost to regulate about the origin when the system starts at any point at any time t can be approximated by the value function,

$$J^* = x^T(t)Px(t) \quad (6)$$

The level sets of this value function describe ellipses in the state space (ellipsoids in systems with more than two states) from which the system can be moved to the origin for a given cost. For linear systems, the Riccati equation solution matrix is constant throughout the entire state space, and therefore the size and orientation of these level sets is constant. If one implements the LQR to control the nominal nonlinear plant eq.(1), the degree to which the intended linear controller performance is realized depends on the extent of nonlinearity of the process. One way to assess this change in performance due to nonlinearity is to add a perturbation term, denoted $\nu(t)$, to the control law,

$$u^*(t) = -R^{-1}B^T Px(t) + \nu(t) \quad (7)$$

in the closed-loop system:

$$\frac{dx}{dt} = f(x(t), u^*(x(t), \nu(t))) \quad (8)$$

The perturbation may be considered as a means of incorporating knowledge of the process nonlinearities in the control law to account for setpoint or load changes. To ascertain the effect of $\nu(t)$ on the performance of the closed-loop system, (6) is differentiated with respect to $\nu(t)$. When the optimal linear controller with perturbation, (7) is applied to the linear system, (2), the resultant closed-loop model is

$$\begin{aligned}\dot{x} &= (A - BR^{-1}B^T P)x(t) + B\nu(t) \\ y(t) &= Cx(t)\end{aligned}\quad (9)$$

The system (9) is a linear system where $\nu(t)$ is an input which is known to enter the solution $x(t)$ linearly:

$$\begin{aligned}x(t) &= x(t_0)e^{(A - BR^{-1}B^T P)(t - t_0)} \\ &+ \int_{t_0}^t \left(e^{(A - BR^{-1}B^T P)(t - \tau)} B\nu(\tau) \right) d\tau\end{aligned}\quad (10)$$

If we consider only constant perturbation, $\nu(t) = \nu$, and we assume that the system starts from the origin, $x(t_0) = 0$, J^* can be evaluated as

$$J^* = \nu^T \tilde{P} \nu$$

where \tilde{P} is formed from the coefficient matrix of $\nu(t)$ in the integrand of (10) and the Riccati equation solution matrix P . J^* may be represented about $\nu = 0$ as a Taylor series polynomial,

$$\begin{aligned}J^*(\nu)|_0 &= J^*(0) + \left. \frac{\partial J^*(\nu)}{\partial \nu} \right|_{\nu=0} \nu + \frac{1}{2!} \left. \frac{\partial^2 J^*(\nu)}{\partial \nu^2} \right|_{\nu=0} \nu^2 \\ &+ \frac{1}{3!} \left. \frac{\partial^3 J^*(\nu)}{\partial \nu^3} \right|_{\nu=0} \nu^3 + \mathcal{O}(4)\end{aligned}\quad (11)$$

where $\mathcal{O}(4)$ is a fourth-order truncation error term. Since J^* is a quadratic function of ν for linear systems, the third-order term, and the truncation error, is exactly zero. Thus, it is possible to assess the effect of nonlinearity on local controller performance by assessing the magnitude of the third-order term in eq.(11). Considering only the magnitude of the third derivative of the value function with respect to the input perturbation is wrought with scaling and dimensionality issues, as $\frac{\partial^3 J^*}{\nu^3}$ has units from η and the inputs. In order to assess the magnitude of the third order term, we propose the following dimensionless quantity, called the performance sensitivity measure (PSM):

$$PSM = \frac{\frac{\partial^3 J^*}{\partial \nu^3}}{\left\| \frac{\partial^2 J^*}{\partial \nu^2} \right\|^{\frac{3}{2}}} \sqrt{J_{min}^*}\quad (12)$$

where J_{min}^* the minimal (quadratic) cost attainable in the particular region of interest. The PSM considers how the cost J^* changes as the process moves along the closed loop locus normalized by the largest cost contour completely contained within the operating region chosen. A small value of the PSM indicates that the nominal linear controller performance is not sensitive to the effect of

the process nonlinearity. In that case, the linear controller provides uniform performance over the region of interest. If the PSM is large then the nonlinearity has a drastic impact of the performance of the linear controller. In general, a PSM value of 1.5 is deemed important as it leads to an average departure of 30% from the nominal linear controller performance.

2.1 PSM of a Nonlinear System

For a nonlinear system, $\nu(t)$ does not enter the solution $x(t)$ linearly, even for control-affine systems, and therefore J^* is not a quadratic value function. Consequently, the Taylor series expansion of J^* given in (11) has a nontrivial third-order coefficient.

For the case where $\nu(t)$ is a constant, the higher order derivatives of $J^*(\nu)$ are computed as follows. The states are assumed to be scaled to nominal operating regions to permit the identity matrix to be employed for Q in the objective function, and R chosen according to the desired control attenuation level. As described above, the optimal linear controller may be found, and the perturbed input, (7), employed. The approximation of the value function is then

$$\begin{aligned}J^* &= \begin{pmatrix} x_1 & \cdots & x_n \end{pmatrix} \begin{pmatrix} P_{1,1} & \cdots & P_{1,n} \\ \vdots & \ddots & \vdots \\ P_{n,1} & \cdots & P_{n,n} \end{pmatrix} \begin{pmatrix} x_1 \\ \vdots \\ x_n \end{pmatrix} \\ &= \sum_{j=1}^n \sum_{i=1}^n x_i P_{i,j} x_j\end{aligned}\quad (13)$$

where x_i , $1 \leq i \leq n$, represents the solution of the perturbed closed-loop system under constant input ν . Differentiating J^* with respect to ν , we obtain

$$\begin{aligned}\frac{\partial J^*}{\partial \nu_l} &= \sum_{i,j=1}^n \left(\frac{\partial x_i}{\partial \nu_l} P_{i,j} x_j + x_i P_{i,j} \frac{\partial x_j}{\partial \nu_l} \right) \\ &= 2 \sum_{i,j=1}^n P_{i,j} \frac{\partial x_i}{\partial \nu_l} x_j,\end{aligned}$$

$$\frac{\partial^2 J^*}{\partial \nu_l \partial \nu_m} = 2 \sum_{i,j=1}^n \left(\frac{\partial^2 x_i}{\partial \nu_l \partial \nu_m} P_{i,j} x_j + \frac{\partial x_i}{\partial \nu_l} P_{i,j} \frac{\partial x_j}{\partial \nu_m} \right),$$

and

$$\begin{aligned} \frac{\partial^3 J^*}{\partial \nu_l \partial \nu_m \partial \nu_k} &= 2 \sum_{i,j=1}^n P_{ij} \left(\frac{\partial^2 x_i}{\partial \nu_l \partial \nu_k} \frac{\partial x_j}{\partial \nu_m} \right. \\ &\left. + \frac{\partial x_i}{\partial \nu_l} \frac{\partial^2 x_j}{\partial \nu_m \partial \nu_k} + \frac{\partial^3 x_j}{\partial \nu_k \partial \nu_l \partial \nu_m} x_i + \frac{\partial^2 x_j}{\partial \nu_l \partial \nu_m} \frac{\partial x_i}{\partial \nu_k} \right) \end{aligned}$$

All the derivatives of J^* are evaluated at $x = 0$ and $\nu = 0$ to obtain a local measure of sensitivity that applies to the closed-loop system operating at its setpoint. The computation of the derivatives of J^* requires the calculation of the 1st, 2nd and 3rd order sensitivity coefficients of $x(t)$ with respect to ν . The sensitivity coefficients are computed by the integration of the sensitivity equations. Due to space restrictions, we omit to list the full set of sensitivities. As an illustration, we consider the derivation of the first order sensitivity equations. Differentiating (1) with respect to ν and inverting the order of differentiation, we obtain

$$\frac{d}{dt} \frac{\partial x}{\partial \nu} = \frac{\partial f}{\partial x} \frac{\partial x}{\partial \nu} + \frac{\partial f}{\partial \nu} \quad (14)$$

Eq.(14) can be integrated along with the perturbed closed-loop system to obtain the first order sensitivity coefficients. In the current development, we consider the trivial solution for $x = 0$ at $\nu = 0$. The same applies to the higher order sensitivity coefficients. Note that the solution of the sensitivity equations yields a time-varying PSM value that we could use to assess the variations in performance as a function of time. Since we focus on the infinite-horizon optimal control problem, it is sufficient to evaluate the steady-state value of the derivatives of J^* with respect to ν at $\nu = 0$. The resulting steady-state PSM provides an estimate of the sensitivity of the infinite horizon cost to small perturbations in the control law. By the local stability of the nominal system under LQR control, the steady-state values of the sensitivity coefficients can be shown to exist and to be finite.

An important consideration is the effect of state scaling on the values of the PSM. Process states with significantly different nominal values affects the PSM through the optimal linear controller gain matrix. It is therefore necessary to scale the states of the system appropriately. Knowledge of the typical range of operation can enable standardization, so that each of the states has zero nominal value and varies within the range $[-1, 1]$:

$$z_i(t) = \frac{x_i(t) - \bar{x}_i(t)}{x_i^{max} - x_i^{min}} \quad (15)$$

In general, such scaling is used to ensure consistency of the analysis over a region of particular interest.

In addition, it is important to note that the current development is not restricted to the LQR. The analysis applies equally to the analysis of sensitivity of an LQG controller or any other linear controller design with quadratic cost performance.

2.2 Example: Chemostat Bioreactor

Consider the model of a chemostat bioreactor (Guay *et al.* 1995):

$$\frac{dx_1}{dt} = \frac{\mu_{max} x_1 x_2}{1 + x_2 + K_i x_2^2} - k_d x_1 - u_1 x_1 \quad (16)$$

$$\frac{dx_2}{dt} = -\frac{\mu_{max} x_1 x_2}{1 + x_2 + K_i x_2^2} + (S_0 - x_2) u_1$$

where x_1 and x_2 are the biomass and substrate concentrations, respectively, in g/L, and u_1 is the dilution rate, in min^{-1} . The model parameters $\mu_{max} = 0.5 \text{ min}^{-1}$, $S_0 = 0.3 \text{ g/L}$, $k_d = 0.05 \text{ min}^{-1}$, and $K_i = 10 \text{ L/g}$ represent the specific growth rate, inlet substrate concentration, death rate and substrate inhibition constant, respectively. The nonlinearity measure proposed in (Guay *et al.* 1995) suggests the process would be the most difficult to control with a linear controller near $(x_1, x_2) = (0.02, 0.2)$.

Consider five points of steady state operation, labelled in Figure 1, chosen by uniformly selecting constant input values in the interval $[0.002, 0.018]$, as shown in Table 2.2.

Point Label	u_{nom}	x_1	x_2
a	0.002	0.00622	0.13826
b	0.006	0.01528	0.15736
c	0.010	0.01982	0.18107
d	0.014	0.01881	0.21403
e	0.018	0.00327	0.28765

Table 2.1. Selected operating points for chemostat bioreactor.

Choosing point ‘‘c’’, the states are scaled about the nominal steady state operating point $(x_1^{nom}, x_2^{nom}) = (0.01982, 0.18107)$, with the ranges chosen as $\tilde{x}_1 \in [x_1^{nom} \pm 0.0025]$, and $\tilde{x}_2 \in [x_2^{nom} \pm 0.025]$. We express

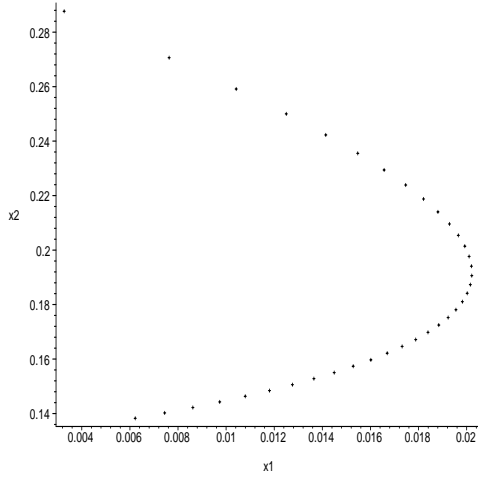


Fig. 1. The steady state locus of the chemostat bioreactor. Points represent the steady states of the system when the input is chosen uniformly in the interval $[0.002, 0.018]$.

the system equations in scaled coordinates and we choose the quadratic performance metric

$$\eta = \int_{t=0}^{\infty} (\tilde{x}^T \tilde{x} + (50u_1)^2) dt$$

Linearizing the system about the origin, corresponding to (2), and solving the corresponding algebraic Riccati equation we obtain the linear quadratic regulator

$$u_1(t) = 0.010 + 0.0069160\tilde{x}_1(t) - 0.024268\tilde{x}_2(t) + \nu(t) \quad (17)$$

For this system, the first and second partial derivatives are found to be

$$\begin{aligned} \frac{\partial \tilde{x}_1}{\partial \nu} &= 29.300 & \frac{\partial \tilde{x}_2}{\partial \nu} &= 38.001 \\ \frac{\partial^2 \tilde{x}_1}{\partial \nu^2} &= -6855.5 & \frac{\partial^2 \tilde{x}_2}{\partial \nu^2} &= -1304.5 \end{aligned}$$

If we pick the operating region to be $\{\tilde{x}_1^2 + \tilde{x}_2^2 \leq 1\}$ then the value of J_{min}^* is simply equal to the minimum eigenvalue of the Riccati equation solution matrix, P . The PSM at point "c" is $PSM = -0.94005$.

To provide an indication of whether the PSM value for point "c" is significant, consider the evaluation of the PSM for the other four points previously identified: The relative PSM values are consistent with results that should be expected from the geometry of the steady state locus

Point Label	u_{nom}	x_1	x_2	PSA
a	0.002	0.00622	0.13826	-0.037179
b	0.006	0.01528	0.15736	-0.13989
c	0.010	0.01982	0.18107	-0.94005
d	0.014	0.01881	0.21403	-0.92211
e	0.018	0.00327	0.28765	0.016861

Table 2.2. Computed PSM values for the five selected points of the chemostat bioreactor.

(see Figure 1). From the actual PSM values computed for the chemostat bioreactor, it is expected that a linear controller could be used without significant deviation in performance about any of the five operating points.

3. EMPIRICAL MEASURES OF CONTROLLER PERFORMANCE

Much of the work in the assessment of process control schemes within the last decade can be traced back to (Harris 1989). Minimum variance benchmarking, as proposed in (Harris 1989), is a widely accepted for the assessment of performance in control systems. In this study, we focus on Harris's controller performance measure for single-input, single-output processes. The reader is referred to (Harris 1989) for more details on the evaluation of the performance measure.

Since the PSM indicates the sensitivity of quadratic system performance of a linear controller, it is reasonable to assume that a large PSM value would also indicate significant variations in a minimum variance benchmarking measure over a particular region of interest. Thus if we design a linear control based on a local linear approximation of the process, the large PSM would indicate that the implementation of the linear controller at other setpoints in the region of interest would result in significant deviations in controller performance measures. In order to evaluate this premise, we consider the chemostat bioreactor model operating at point "c" in closed-loop with the LQR control eq.(17) (with $\nu(t) = 0$). In order to proceed with the assessment of controller performance, we consider the biomass concentration as the measured output. Furthermore, we corrupt the measurements with uncorrelated white noise, $a(t)$ passed through the discrete transfer function

$$\frac{1}{1 + 0.4z^{-1}}$$

The noise power is set to 0.001, chosen to ensure that the closed-loop deviation from steady state is less than one in magnitude, meaning the process remains in the region suggested by the scaling of Section 2.2. The process was simulated for 400 minutes, with a fixed step-size of 0.1 minutes. For this process, Harris' minimum variance benchmark $\eta(0)$ was 0.15 for the regulation of the system at point "c". This value indicates that only 15% of current output variance could be eliminated through use of a minimum variance controller. Thus the linear control operates well in this region.

The strategy is to implement the linear controller developed under the conditions at point "c" at different setpoints. To move the process about the operating region along the closed-loop locus, a constant perturbation, $\nu(t)$ is input to the system which is then allowed to reach the new steady state. An equivalent way to handle this problem would be to assign setpoints along the steady-state locus. By evaluating the controller performance measure about each setpoint we obtain an estimate of the sensitivity linear controller performance to the location of the setpoint. It is clear that if the plant is linear then the performance measure remains essentially unchanged over the region of interest. Therefore, this relatively simple exercise provides a potential substitute to the PSM for operating control systems. It remains to show that the interpretation of the PSM provides a good indication of the sensitivity of linear control performance.

Table 3 shows the perturbed steady state values, and the minimum variance performance measure found at each of the points. Although the closed loop gains vary through-

Point Label	$\nu(t)$	\tilde{x}_1	\tilde{x}_2	$\eta(0)$
c+++	0.008	0.072274	0.27352	0.1629
c++	0.004	0.070454	0.14320	0.1630
c+	0.002	0.045610	0.073582	0.1631
c	0	0	0	0.1631
c-	-0.002	-0.074435	-0.078981	0.1631
c-	-0.004	-0.18670	-0.16527	0.1632
c-	-0.008	-0.63025	-0.38039	0.1618

Table 3.3. Perturbed operating points for chemostat bioreactor about point "c".

out the region considered, there is very little change in performance. In fact, the variability is insignificant given the computations required to compute $\eta(0)$. The operating region about point "c" is unsusceptible to perfor-

mance degradation from closed loop nonlinearity and therefore a linear, finite gain controller performs well throughout.

4. CONCLUSIONS

The performance sensitivity array has been introduced as a closed-loop measure that attempts to quantify the effect of nonlinearity on the performance of a nonlinear system subject to a linear quadratic regulator. The results demonstrate that the PSM can be used to predict the linear controller performance on nonlinear systems. Its impact can be verified by considering a simple minimum variance benchmarking approach.

REFERENCES

- Allgöwer, F. (1995a). Definition and computation of a nonlinearity measure. *IFAC Nonlinear Control Systems Design* pp. 257–262.
- Allgöwer, F. (1995b). Definition and computation of a nonlinearity measure and application to approximate i/o-linearization. Technical report. Universität Stuttgart.
- Desoer, C.A. and Y.-T. Wang (1981). Foundations of feedback theory for nonlinear dynamical systems. *IEEE Transactions on Circuits and Systems* (2), 104–123.
- Guay, M., P.J. McLellan and D.W. Bacon (1995). Measurement of nonlinearity in chemical process control systems: The steady state map. *The Canadian Journal of Chemical Engineering* **73**, 868–882.
- Haber, R. (1985). Nonlinearity tests for dynamic processes. *IFAC Identification and System Parameter Estimation* pp. 409–414.
- Harris, T.J. (1989). Assessment of control loop performance. *The Canadian Journal of Chemical Engineering* **67**, 856–861.
- Ogunnaike, B.A., R.K. Pearson and F.J. Doyle III (1993). Chemical process characterization: Applications in the rational selection of control strategies. *Proc. Europ. Cont. Conf., June 28–July 1* pp. 1067–1071.
- Stack, A.J. and F.J. Doyle III (1997). The optimal control structure: An approach to measuring control-law nonlinearity. **21**(9), 1009–1019.

APPLICATION OF SOFTWARE SENSORS FOR MONITORING AND PREDICTION IN FERMENTATION PROCESSES

Mads Thaysen ^{*,**,1} Sten Bay Jørgensen ^{**}

** BioProcess Laboratories, Novo Nordisk A/S,
Hagedornsvej 1, HAB 2.35, 2800 Gentofte, Denmark*

*** CAPEC, Department of Chemical Engineering,
Technical University of Denmark*

Abstract: The development of modelbased process software sensors for monitoring of biomass concentration and product concentration in fed-batch and continuous yeast fermentations is presented, followed by a validation of the sensors using data from industrial fermentations. Alternatively, using multiway projection to latent structures (MPLS) algorithm, a model for prediction of one-step ahead and end point product concentrations is developed and demonstrated on industrial process data. The one-step ahead MPLS-predictor is compared to the modelbased product concentration software sensor. The comparison indicates a better performance by the MPLS-predictor. *Copyright ©2003 IFAC*

Keywords: Process software sensors, MPLS, prediction, industrial process data.

1. INTRODUCTION

To improve monitoring and control of industrial fermentation processes it is desirable to include interpreted information of dynamic responses of relevant biological and chemical species to changes in process conditions whenever possible. Fulfilling this desire is however not trivial, since measurements of relevant species often are difficult to conduct and often impossible to obtain at the desired rate. An alternative approach to the direct measurement of species is the development of process software sensors based on mathematical models correlating measurable variables to the desired variables. This work will develop two different types of software sensors, one based upon first principles engineering modelling and another based upon chemometrics.

2. PROCESS SOFTWARE SENSORS

First principles engineering models (FP-EM) can form the underlying foundation for software sensors. The models infer information of unmeasured entities by using available information from other measured entities. Different frameworks can be used for the model development. First software sensors using FP-EMs will be developed and investigated for the prediction of biomass and peptide product concentration in a fermentation broth. Subsequently a chemometric model is used for developing a software sensor for product estimation. Finally the two types of product concentration sensors are compared.

2.1 FP-EM based Sensor for Biomass Concentration

Lei (2001) and others demonstrated that it was possible to use a component mass balance on the proton production or consumption rate in a high

¹ Partially supported by the Academy of Technical Sciences, Denmark

performance laboratory setup to obtain a simple on-line estimation of the biomass concentration in batch, fed-batch and continuous fermentation of *Saccharomyces cerevisiae*.

A simplified illustration of the contributions to the proton balance in a bioreactor is shown in figure 1. A component mass balance for the proton concentration $[H^+]$ in the extracellular medium yields:

$$V \frac{d[H^+]}{dt} = F_s[H^+]_{s,in} - F_e[H^+]_{e,out} + F_{H^+,gen} - F_{NH_3} \quad (1)$$

where the dual role of NH_3 is i) to maintain a constant pH-level in the medium and ii) to act as the primary nitrogen source for biomass production.

The following assumptions are used for simplification of the mass balance expression:

- Constant pH-level in the bioreactor
- Negligible contribution to proton balance from pH-diff. between feed and medium pH

In the original work the pH of the feed was adjusted to the pH of the medium. In this work estimation of the amount of proton equivalents needed to compensate for this pH-difference indicated that less than 1% of the molar flow of NH_3 is needed to balance the pH-difference between feed and medium pH.

The simplified mass balance yields:

$$0 = F_{H^+,gen} - F_{NH_3} \quad (2)$$

The volumetric proton production rate can now be calculated as:

$$r_{H^+} = \frac{F_{H^+,gen}}{V} = \frac{F_{NH_3}}{V} \quad (3)$$

The following assumptions have been made concerning possible sources contributing to the proton production rate from cellular activities during aerobic growth on a complex medium:

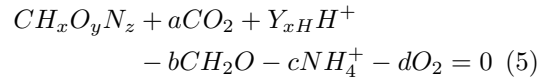
- Uptake of NH_4^+ as primary nitrogen source
- Negligible production or consumption of organic acids
- Negligible consumption of amino acids from complex medium
- No acidification of the medium due to production of CO_2

During aerobic growth on glucose only negligible amounts of organic acids are produced; CO_2 and biomass being the primary carbon-products formed. Contribution to the proton balance by the solution and dissociation of H_2CO_3 to carbonate can be disregarded when the pH-level is significantly below pH 7. By further assuming only negligible consumption of organic N-sources from the complex medium, the uptake of NH_4^+ is the only contributor to the proton production rate and the only significant nitrogen source. A 1:1 ratio between proton production rate and the NH_4^+ uptake rate (using has been observed indicating that the biomass production rate is proportional to the proton production rate, under the assumption that the nitrogen content of the biomass to be constant during balanced growth.

Based on the above comments and assumptions the volumetric biomass production rate, $r_x^{H^+}$, can be calculated from volumetric NH_3 addition rate:

$$r_x^{H^+} = \frac{M_{DW} \cdot r_{H^+}}{Y_{xH}} = \frac{M_{DW} \cdot F_{NH_3}}{Y_{xH} \cdot V} \quad (4)$$

with M_{DW} as the molar weight of dry weight biomass and Y_{xH} is the yield coefficient of mole protons produced per mole biomass i.e. the molar content of nitrogen in biomass based on the overall growth stoichiometry:



From the stoichiometric equation it can be seen that Y_{xH} is constant, since NH_4^+ is the only proton source and $z = c (= Y_{xH})$ since NH_4^+ is the only nitrogen source. Combination of the above expressions with a dynamic mass balance for biomass (x):

$$\frac{dx}{dt} = r_x - Dx \quad (6)$$

yields a simple biomass predictor:

$$x_{k+1} = x_k \cdot \exp\left(\left(\frac{r_{x_k}^{H^+}}{x_k} - D_k\right)(t_{k+1} - t_k)\right) \quad (7)$$

where D_k is the dilution rate at time point t_k .

The above model has been developed assuming ideal conditions in fermentor. Both for small and large scale fermentations with high cell densities this assumption is unlikely to be valid. To account for these variations the model has been modified as follows:

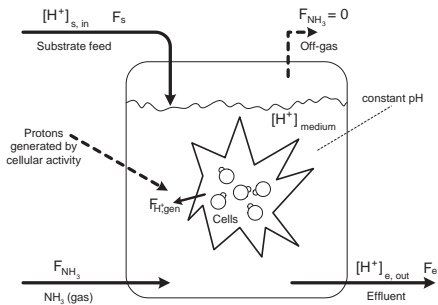


Fig. 1. Simplified schematic illustration of flows and factors that influence the extracellular proton concentration balance in the fermentation medium.

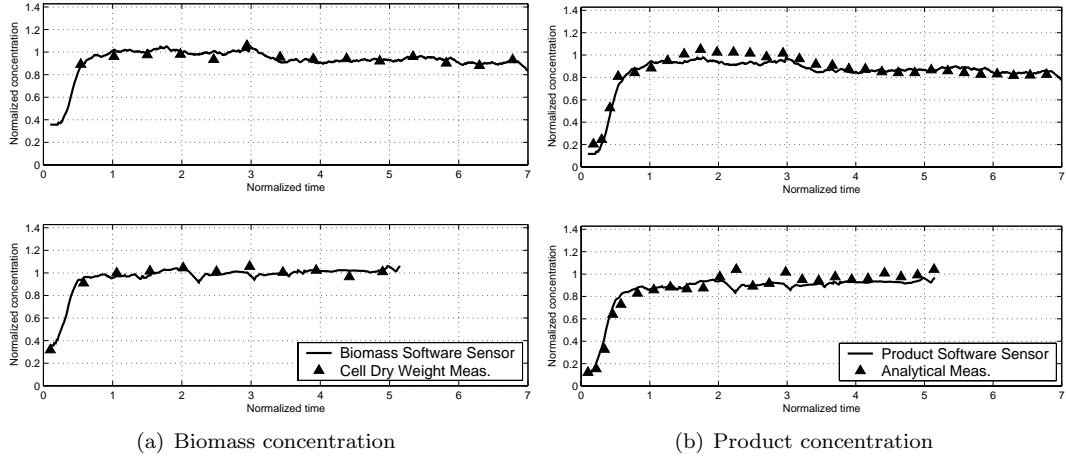


Fig. 2. Comparison of signals from software sensors (—) and analytical measurements (▲) for fermentations in two different fermentors.

$$x_{k+1} = x_k \cdot \exp\left(\left(\frac{\alpha \cdot F_{NH_3,k}}{V_k \cdot x_k} - D_k\right)(t_{k+1} - t_k)\right) \quad (8)$$

where $\alpha = f(t, M_{DW}, Y_{xH}, \text{vessel properties})$ is determined for the individual fermentor.

Two examples of the application in simulation of the biomass concentration software sensor are illustrated in figure 2(a).

2.2 FPEM based Sensor for Product Concentration

To develop a process software sensor for prediction to the peptide product concentration, physiological knowledge of the recombinant yeast strain is used. It is known that the control of the promotor for transcription of the product gene is linked to the activity of the glycolysis of the recombinant strain. To simplify the model formulation the following assumptions are made:

- Production rate of product (r_p) proportional to production rate of biomass (r_x)
- High stability of recombinant gene
- No influence from transport and folding in organelles on production rate
- Effective excretion of product

A high stability of the recombinant gene ensures that no decay in specific productivity of the peptide product is experienced over time. Furthermore by assuming that the transport of the peptide product through the organelles of the cell does not seem to have any influence on the production rate, combined with effective folding and excretion of the peptide product to the abiotic phase, the rate limiting step of the cellular production process becomes transcription of the recombinant gene.

Based on the above assumptions the following model for the production rate of the product (p)

is proposed:

$$r_p \propto r_x = \frac{M_{DW} \cdot F_{NH_3}}{Y_{xH} \cdot V} \quad (9)$$

Introducing a parameter (β) accounting for the issues relating to non-ideal process conditions and variations in growth stoichiometry (Y_{xH}) and cell composition (M_{DW}) a dynamic mass balance on the product becomes:

$$\frac{dp}{dt} = r_p - Dp = \beta \frac{F_{NH_3}}{V} - Dp \quad (10)$$

leading to the product predictor:

$$p_{k+1} = p_k \cdot \exp\left(\left(\frac{\beta \cdot F_{NH_3,k}}{V_k \cdot p_k} - D_k\right)(t_{k+1} - t_k)\right) \quad (11)$$

where $\beta = g(t, M_{DW}, Y_{xH}, \text{vessel properties})$ is determined for the individual fermentor.

Two examples of the application in simulation of the product concentration software sensor are illustrated in figure 2(b) along with signals from biomass concentration software sensors from the same fermentations. The software sensors are activated after the batch phase and used for the fed-batch and continuous phases of the fermentation with constant β values.

2.3 Multiway Projection to Latent Structures (MPLS)

Process monitoring and prediction of end quality using MPLS have been illustrated by a number of research groups e.g. Nomikos and MacGregor (1995). The general idea behind MPLS is that an empirical model is build on measurements from reference batches operated under normal operating conditions producing a good quality product in terms of high concentration. This work has focused on the prediction possibilities of the MPLS. The available on-line measurements are used to estimate or predict product quality, which

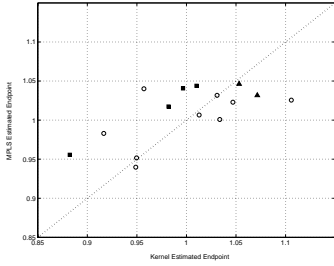


Fig. 3. Product concentrations at end of batch estimated using MPLS and kernel estimators. (○) M-, (▲) V- and (■) A-batches.

is desirable, since a limited number of analytical measurements of the quality variables is available in an off-line fashion. The on-line measurements are arranged in an array \mathbf{X} and the quality measurements are arranged in another array \mathbf{Y} .

Using the MPLS-algorithm a regression equation can be formulated:

$$\hat{\mathbf{Y}} = \mathbf{X}\mathbf{B}, \text{ with } \mathbf{B} = \mathbf{W}(\mathbf{P}^T\mathbf{W})^{-1}\mathbf{Q}^T \quad (12)$$

This regression model \mathbf{B} can then be used for on-line prediction of the end quality of the batch provided that a suitable method for the estimation of future on-line measurements is available (Nomikos and MacGregor, 1995). This work has been applying the method using the J measurements obtained at the last sampling number k to fill in the empty spaces.

The number of PLS-components (C) necessary to obtain a desired level of regression can be evaluated using different methods of (cross-)validation techniques. In this work the root mean square error of prediction ($RMSEP$) is used:

$$RMSEP = \sqrt{\frac{1}{K} \sum_{k=1}^K (\hat{y}_k - y_k)^2} \quad (13)$$

For increasing numbers of PLS-components C used for model identification the $RMSEP$ is evaluated on validation data, where the lowest value of $RMSEP$ indicates the number of PLS-components C to be used.

2.4 MPLS for On-line Prediction and Estimation

In the case where quality measurements are taken frequently during the batch run, the MPLS-framework can be used for estimation and prediction of the intra-batch quality. For all the batches considered in this work, both on-line measurements and off-line quality measurements in each batch have been subsampled to the same frequency by applying a kernel estimator for smoothing using a tricubic kernel with a local linear fit of 3 nearest neighbors (Hastie *et*

Table 1. Exp. var. of \mathbf{X} and \mathbf{Y} . Mean $RMSEP$ from the validation.

Expl. var	No	of	PLS	Comp	
	1	2	3	4	5
\mathbf{X}	16.3	27.4	43.9	56.3	65.2
\mathbf{Y}	56.9	73.1	80.7	86.5	94.4
$RMSEP$	0.039	0.056	0.061	0.060	0.083

al., 2001). With the smoothed data a \mathbf{Y} array is obtained. At sample number k in a new batch the full batch profiles of the quality variables \hat{Y}_k can be obtained by filling in the empty spaces in X_k as described above and applying the regression matrix \mathbf{B} :

$$\hat{Y}_k = X_k\mathbf{B} \quad (14)$$

2.5 MPLS Applied on Industrial Data

In this work the only quality variable to be regressed was the product concentration. 11 on-line measured variables were sampled 180 times during a fermentation, operating in fed-batch phase followed by a continuous phase. 9 batches conducted under normal operating conditions were used for the model identification (M-batches), while 2 validation batches (V-batches) were used to determine the number of PLS-components to be included in the model evaluated by the $RMSEP$ as describe above. The explained variance and $RMSEP$ for the 5 first PLS-components are shown in table 1. It is interesting to note that the $RMSEP$ evaluation indicates that only 1 PLS-component should be included in the model, explaining 55 % of the variation in \mathbf{Y} .

The model performance was then investigated using the 2 V-batches along with 4 additional batches (A-batches), the latters having normal end-point concentrations of the product, but undergoing small process upsets during operation. A comparison between the MPLS estimated and kernel estimated product concentration at the end of the batch is shown in figure 3. The latter of the two estimators is comparable to the analytical measurements. From the figure it is seen how the MPLS estimations at worst are within 10 % of the kernel estimated values for model, validation and A-batches. It is interesting to notice how the MPLS estimations of 4 A-batches all are larger than the kernel estimations.

Figure 4(a) shows the prediction results for a V-batch. A good description of the variations in the kernel estimation and the analytical measurements can be seen by the one-step ahead MPLS-prediction. From time 1.4 and to the end of the batch some variations in both the one-step ahead and end point prediction (starting at coordinates (0,1)) can be noticed. The variations are explained

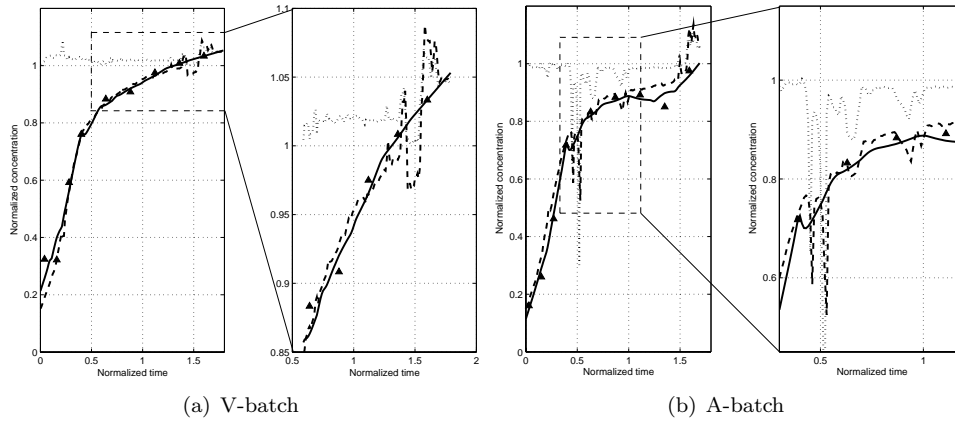


Fig. 4. MPLS product concentration predictions in a validation batch (a) and in batch with a process operation upset (b). (—) kernel estimation, (\blacktriangle) analytical measurements, (---) one-step ahead prediction and (\cdots) batch end prediction.

by a temporary outfall (time 1.4-1.6) of the mass spectroscopy instrument measuring the contents in the off-gas from the fermenter. The effects of the disturbance are seen to have settled at the end of the batch.

The predictions of the MPLS-model in one of the A-batches where a small upset in the process operation occurs are illustrated in figure 4(b). The first upset occurs at time 0.4, where the fermentation is stopped because a fault has occurred in the ammonia supply system. A number of actions occur as a consequence of this fault, resulting in large variations in the one-step ahead prediction and the end concentration prediction. A general decrease in the end point concentration is seen until the system is fully returned to normal operating conditions at time 0.7.

At time 0.9 a new disturbance appears, this time the substrate flow is stopped for a while. Both predictions decrease with this change, but are restored to normal after the substrate flow is reinitiated at time 1.0.

The one-step ahead predictor is very close for all but one of the analytical measurements. Also the kernel estimated product concentration lies in general close to the one-step ahead predictor. However at the end of the batch both of the predictors are seen to sharply increase their predictions around time 1.6, the reason being a decrease in the dilution rate.

Figure 5 shows prediction error between the kernel estimated concentration and the analytical measurements and the one-step ahead prediction respectively. The prediction errors are illustrated for the 2 V-batches (top left and right) and the 4 A-batches, where the dotted lines represent the $\pm 10\%$ value of the kernel estimation. For 5 of 6 batches (not middle right) it is seen how the MPLS-predicted end concentrations are within $\pm 10\%$ of the final product concentration thus indicating that even with possible process upsets the predicted end point concentration was good.

3. PERFORMANCE COMPARISON OF FPEM- VERSUS MPLS-PREDICTOR

In the above two methods for one-step ahead prediction of the product concentration have been developed and tested. Figure 6 shows the prediction error between the kernel estimated concentration and the analytical measurements, the one-step ahead MPLS-predictor and the FPEM-predictor (product concentration software sensor) respectively. It can be seen that the MPLS-predictor to some degree is able to capture the values of the analytical measurements and the kernel estimations between the data points. However after approximately 20% of the batch time, the predictions are within 10% of the analytical measurements during normal operation. The MPLS-predictor performs better than the FPEM-predictor, which in general can be seen to have big positive errors in the first

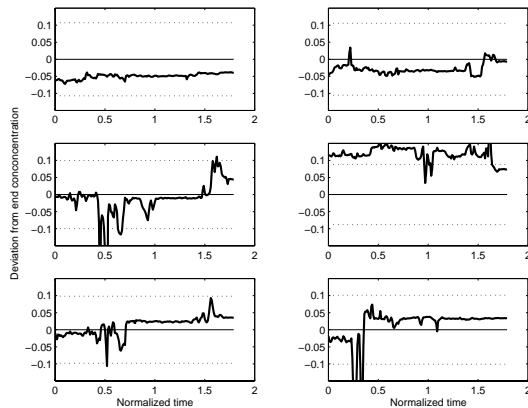


Fig. 5. Prediction error of end point product concentration in 2 V-batches (top) and 4 A-batches. (—) MPLS-prediction and (\cdots) $\pm 10\%$ errors of the kernel est. end value.

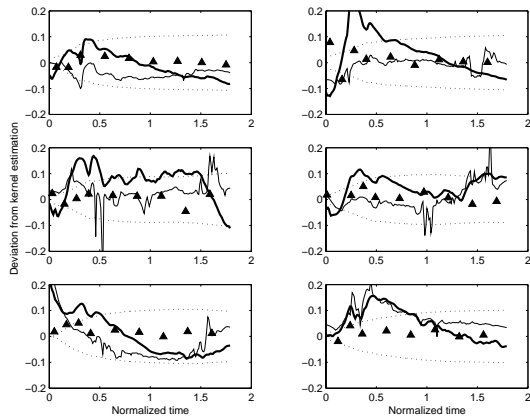


Fig. 6. Prediction errors between kernel est. values and one-step ahead product concentration predictors. MPLS-predictor (—) and FPEM-predictor (—, bold) in 2 V-batches (top) and 4 A-batches. (▲) analytical measurements and (··) $\pm 10\%$ on the kernel est. values.

quarter of the batch, approximately corresponding to the fed-batch phase. This is not desirable, since it is in the non-stationary phases that accurate and precise estimation and prediction is most important from an optimization perspective.

To support the comparison, *RMSEP* values have been calculated in different phases of the fermentation process and shown in table 2. The FPEM-predictor can be seen to have relatively large errors in the first part of the batch corresponding to the fed-batch phase. While the *RMSEP* of the MPLS-predictor also is the largest in the fed-batch phase, the predictor still performs well. In the stationary phase (phase 3) the results of the two predictors are approximately the same.

4. DISCUSSION AND CONCLUSION

In this paper two different methods for obtaining quantitative information from a fermentation process has been presented and preliminarily compared. The methods have been applied using on-line process data from an industrial fermentation process to illustrate the type and quality of information obtainable with the methods.

A software sensor was developed for monitoring of the biomass concentration and was based on FPEMs using the feed rate of ammonia, volume of broth and the dilution rate as inputs. Application of the software sensor using on-line process data gave a good description of the variations seen in the analytical measurements, leading to the

Table 2. Mean *RMSEP* of phases.

Phase	1	2	3	Total
Time	0.0 - 0.5	0.5 - 1.0	1.0 - 1.8	0.0 - 1.8
FPEM	0.039	0.027	0.022	0.030
MPLS	0.025	0.021	0.021	0.023

conclusion that the implementation of this device will enable on-line monitoring of the biomass concentration.

A similar software sensor was then developed for monitoring of the product concentration using the same framework as the biomass concentration software sensor. Although complex cellular processes are involved in the processes for generating the peptide a very simple model was developed by only slightly modifying the FPEM used for modelling the biomass concentration. Applied on the industrial data this simple software sensor was also able to give a good description of the general product concentration trajectory making on-line monitoring of the product concentration possible if implemented.

An alternative approach for monitoring component concentrations in a process is through process chemometrics. A model for predicting the product concentration based on the MPLS-algorithm was developed producing a linear model describing changes around an average trajectory. The model was tested on the industrial data and indicated that both one-step ahead and end point predictions of the product concentrations came within 5-10 % of the kernel estimated values based on analytical measurements.

The MPLS-predictor for the one-step ahead prediction was compared with the simple product concentration software sensor (FPEM-predictor), where the first gave a more accurate description of the variations in the product concentration.

In conclusion this work has provided insight into tools for monitoring a given fermentation process with respect to biomass concentration and product concentration. Areas to address in future work is the trade off between bias and variance in on-line estimators, the use of available analytical measurements for parameter adaption, development of a better description of the dynamics of product formation and extending the application of the MPLS-algorithm.

REFERENCES

- Hastie, Trevor, Robert Tibshirani and Jerome Friedman (2001). *The Elements of Statistical Learning. Data Mining, Inference and Prediction..* Springer Verlag, New York.
- Lei, F. (2001). Dynamics and non-linear phenomena in continuous cultivations of *Saccharomyces cerevisiae..* PhD thesis. KT, Technical University of Denmark.
- Nomikos, Paul and John F. MacGregor (1995). Multivariate SPC charts for monitoring batch processes. *Technometrics* **37**(1), 41–59.